

RESEARCH ARTICLE

EBV miRNAs are potent effectors of tumor cell transcriptome remodeling in promoting immune escape

Nathan Ungerleider¹, Whitney Bullard², Mehmet Kara², Xia Wang¹, Claire Roberts¹, Rolf Renne², Scott Tibbetts^{2*}, Erik K. Flemington^{1*}

1 Department of Pathology, Tulane University School of Medicine, Tulane Cancer Center, New Orleans, Louisiana, United States of America, **2** Department of Molecular Genetics and Microbiology, UF Health Cancer Center, University of Florida, Gainesville, Florida, United States of America

* stibbe@ufl.edu (ST); erik@tulane.edu (EKF)



OPEN ACCESS

Citation: Ungerleider N, Bullard W, Kara M, Wang X, Roberts C, Renne R, et al. (2021) EBV miRNAs are potent effectors of tumor cell transcriptome remodeling in promoting immune escape. *PLoS Pathog* 17(5): e1009217. <https://doi.org/10.1371/journal.ppat.1009217>

Editor: Shou-Jiang Gao, UPMC Hillman Cancer Center, UNITED STATES

Received: December 16, 2020

Accepted: April 15, 2021

Published: May 6, 2021

Copyright: © 2021 Ungerleider et al. This is an open access article distributed under the terms of the [Creative Commons Attribution License](https://creativecommons.org/licenses/by/4.0/), which permits unrestricted use, distribution, and reproduction in any medium, provided the original author and source are credited.

Data Availability Statement: All source code is available in our GitHub repository (https://github.com/flemingtonlab/ebv_clash) Small fraction and CLASH sequences have been deposited to the NCBI Gene Expression Omnibus (GSE147228). Accession numbers for polyA-selected RNA sequencing reads are GSM1267812 (Akata) and GSM1104509 (SNU719).

Funding: This work was supported by the National Institutes of Health [R01CA243793, R21CA236549 to E.K.F., P01CA214091 to E.K.F., S.T., R.R.], and

Abstract

The Epstein Barr virus (EBV) contributes to the tumor phenotype through a limited set of primarily non-coding viral RNAs, including 31 mature miRNAs. Here we investigated the impact of EBV miRNAs on remodeling the tumor cell transcriptome. Strikingly, EBV miRNAs displayed exceptionally abundant expression in primary EBV-associated Burkitt's Lymphomas (BLs) and Gastric Carcinomas (GCs). To investigate viral miRNA targeting, we used the high-resolution approach, CLASH in GC and BL cell models. Affinity constant calculations of targeting efficacies for CLASH hits showed that viral miRNAs bind their targets more effectively than their host counterparts, as did Kaposi's sarcoma-associated herpesvirus (KSHV) and murine gammaherpesvirus 68 (MHV68) miRNAs. Using public BL and GC RNA-seq datasets, we found that high EBV miRNA targeting efficacies translates to enhanced reduction of target expression. Pathway analysis of high efficacy EBV miRNA targets showed enrichment for innate and adaptive immune responses. Inhibition of the immune response by EBV miRNAs was functionally validated *in vivo* through the finding of inverse correlations between EBV miRNAs and immune cell infiltration and T-cell diversity in BL and GC datasets. Together, this study demonstrates that EBV miRNAs are potent effectors of the tumor transcriptome that play a role in suppressing host immune response.

Author summary

Burkitt's Lymphoma and gastric cancer are both associated with EBV, a prolific DNA tumor virus that latently resides in nearly all human beings. Despite mostly restricting viral gene expression to noncoding RNAs, EBV has important influences on the fitness of infected tumor cells. Here, we show that the miRNA class of viral noncoding RNAs are a major viral contributor to remodeling the tumor cell regulatory machinery in patient tumor samples. First, an assessment of miRNA expression in clinical tumor samples showed that EBV miRNAs are expressed at unexpectedly high levels relative to cell miRNAs. Using a highly specific miRNA target identification approach, CLASH, we

the Lymphoma Research Foundation (N.U.). The funders had no role in study design, data collection and analysis, decision to publish, or preparation of the manuscript.

Competing interests: The authors have declared that no competing interests exist.

comprehensively identified both viral and cellular miRNA targets and the relative abundance of each miRNA-mRNA interaction. We also show that viral miRNAs bind to and alter the expression of their mRNA targets more effectively than their cellular miRNA counterparts. Pathway analysis of the most effectively targeted mRNAs revealed enrichment of immune signaling pathways and we show a corresponding inverse correlation between EBV miRNA expression and infiltrating immune cells in EBV positive primary tumors. Altogether, this study shows that EBV miRNAs are key regulators of the tumor cell phenotype and the immune cell microenvironment.

Introduction

The Epstein Barr Virus (EBV) is a ubiquitous gammaherpesvirus (γ HV) that establishes life-long infections in over 90% of the world's population. Since its discovery as the major etiological agent of endemic Burkitt's lymphoma (BL)[1], EBV has been causally associated with other malignancies including NK/T cell lymphoma[2], diffuse large B cell lymphoma[3], Hodgkin's lymphoma[4], nasopharyngeal carcinoma[5] and gastric carcinoma (GC)[6]. Arising from infected founder cells, these tumors maintain a dependence on the virus as they progress[7].

γ HVs utilize two distinct strategies, referred to as lytic and latent replication, to expand the infected host cell population[8]. The lytic replication program is a process utilized by all viruses to replicate and package their genetic content for spread through cell-to-cell transfer. This strategy produces a large number of virions but it destroys the host cell and triggers a strong local immune response[9]. The viral latency program, the phase most closely linked with cancer, is associated with the expression of a small number of genes that support the growth and health of the infected cell[10–16] and by extension, the growth and health of its viral occupant. In this phase of the virus infection cycle, viral and host genomes are replicated concordantly and distributed to daughter cells[17], resulting in an expansion of the infected cell population that is independent of virion production. This form of intracellular replication minimizes immune reactivity, allowing the virus to discretely double the pool of infected cells at each mitotic cycle.

In EBV-associated BLs and GCs, the latency gene expression program is especially restrictive, with the only ubiquitous and consistently expressed viral protein being the replicative factor, EBNA1[18]. More abundantly expressed are a group of viral noncoding RNAs that allow the virus to modulate the host cell environment without eliciting a strong adaptive immune response. These include two short noncoding RNAs (EBER1 and EBER2)[19], a long noncoding RNA (RPMS1)[20], circular RNAs[21,22], and the viral miRNAs[23].

MiRNAs function by targeting complementary mRNAs for destruction[24]. By interacting with an average of 90 unique transcripts[25], a single miRNA can have a substantial impact on the cellular transcriptome[26–30]. The genomes of EBV, KSHV, and MHV68 potentially encode 44, 25, and 28 miRNAs[31–34], theoretically endowing these viruses with the capacity to control nearly every pathway in the cell. Several previous studies have used broad-scale approaches such as AGO-CLIP to uncover viral miRNA targets[35–37], and some of these miRNA-target interactions have since been shown to interrupt apoptosis[38], prevent reactivation[39], and block interferon signaling[40]. The AGO-CLIP approach, however, requires bioinformatic inferences to determine miRNA-mRNA pairings, precluding analysis of binding efficacy and limiting detection to canonical interactions. Here we used a modified version of a more comprehensive and quantitative approach, Crosslinking, Ligation, and Sequencing of Hybrids (CLASH)[41], called qCLASH[42], to broadly uncover *bona fide* targets of EBV

miRNAs. Through integration of mRNA, miRNA, and hybrid abundances, we examine the global binding properties and targeting efficacies inherent to γ HV miRNAs. Assessing pathway enrichment of the highest targeting efficacy EBV miRNA-target interactions shows enrichment for innate and adaptive immune responses. Utilizing clinical BL and GC datasets, we explore the roles of EBV miRNAs in primary tumors and demonstrate a role for EBV miRNAs in dampening the immune response to viral infection and oncogenesis.

Materials and methods

Cell culture

Akata (obtained from Kenzo Takada) and SNU719 (Korean Cell Line Bank) cells were grown in RPMI 1640 media (ThermoFisher Scientific, catalog no. SH30027) supplemented with 10% fetal bovine serum (FBS; ThermoFisher Scientific, catalog no. 10437), and incubated at 37°C in 5% CO₂.

Clinical data

Aligned RNA and miRNA sequencing reads, deposited by the BLGSP and TCGA, were downloaded from the Genomic Data Commons (GDC)[43]. RNA sequencing alignments were converted to FASTQ format using the following command:

```
samtools sort -@ 19 -n $bamfile | samtools fastq -@ 19-1 $fq1-2 $fq2-0 /dev/null -s /dev/null -n -F 0x900 -
```

The resulting raw sequencing reads were pseudoaligned to the human (GENCODE GRCh38.p13)[44] and EBV[45] transcriptomes using kallisto v0.46.0[46] (including the “-rf-stranded” flag for BL sequencing reads, which were strand-specific). The underlying counts or transcripts per million (t.p.m.) values were summed and assigned to each gene. BL analysis was restricted to the “Discovery” cohort due to the reported higher RNA sequencing quality of these samples[47]. With the exception of S1 Fig, GC analysis was restricted to microsatellite stable samples[48].

Aligned miRNA sequencing reads were converted to FASTQ format using the following command:

```
samtools fastq -F 0x900 $bamfile
```

Raw miRNA sequencing reads were aligned to an index of mature human and EBV miRNA sequences (miRbase v22) via bowtie with the following command:

```
bowtie $mir_index -n 3 -m 10 --best --strata -p 10 -S $mir_fastq
```

UV Crosslinking

qCLASH was performed as previously described¹, with 3 biological replicates processed for each cell line. SNU719 cells were trypsinized, resuspended in RPMI 1640 plus 10% FBS, then washed twice with PBS. Akata cells were washed twice with PBS. Both cell lines were resuspended in 10 mL PBS then crosslinked with 250 nm λ UV light for a total exposure of 600J/cm². 50 million cells were transferred to a 1.5 mL tube, pelleted at 800 x g for 5 minutes, and stored at -80°C before processing as described below.

Cell lysis

Cell pellets were thawed and resuspended in 500 μ L cell lysis buffer (50 mM HEPES (pH 7.5), 150 mM KCl, 2mM EDTA, 1mM NaF, 0.5% NP-40, 0.5 mM DTT, and 1x protease inhibitor cocktail (Roche, catalog no. 11836170001)). Cells were lysed for 15 minutes on ice then treated with 10 μ L of RQ1 DNase (Promega, catalog no. M610A) for 5 minutes at 37°C, while shaking

at 1,000 rpm. Lysates were cleared by a 21,000 x g centrifugation for 15 minutes at 4°C. Supernatants were treated for 15 minutes with 0.5 µl RNase T1 (ThermoFisher Scientific, catalog no. EN054) at 22°C.

Preparation of Protein G beads

6 mg of Protein G Dynabeads (Invitrogen, catalog no. 1004D) were washed 3 times then resuspended in PBST (137 mM NaCl, 2.7 mM KCl, 10 mM Na₂HPO₄, 1.8 mM KH₂PO₄, 0.1% (w/v) Tween 20 (pH 7.2)). A final concentration of 200 µg/ml of AffiniPure rabbit α-mouse IgG (Jackson ImmunoResearch, catalog no. 315-005-008) was added and beads were incubated on a rotator for 50 minutes at 25°C. The complexes were washed 3 times with PBST (5 minutes each), then resuspended in 1 mL of PBST. 10 µg of pan-AGO antibody (gift from Zissimos Mourelatos) was added and samples were rotated for 16 hours at 4°C. Beads were then washed 4 times with wash buffer (1x PBS, 0.1% SDS, 0.5% sodium deoxycholate, and 0.5% NP-40).

Immunoprecipitation

1 mL of crosslinked cell lysate was added to the pelleted α-AGO beads. Tubes were put on a rotator and incubated for 16 hours at 4°C. The bead complexes were then centrifuged and washed 3 times with cell lysis buffer, followed by 4 times each with 1x PXL (1x PBS, 0.1% SDS, 0.5% sodium deoxycholate, 0.5% NP-40), 5x PXL (5x PBS, 0.1% SDS, 0.5% sodium deoxycholate, 0.5% NP-40), high-stringency wash buffer (15 mM Tris-HCl (pH 7.5), 5 mM EDTA, 2.5 mM EGTA, 1% Triton X-100, 1% sodium deoxycholate, 0.1% SDS, 120 mM NaCl, 25 mM KCl), high salt wash buffer (15 mM Tris-HCl (pH 7.5), 5 mM EDTA, 2.5 mM EGTA, 1% Triton X-100, 1% sodium deoxycholate, 0.1% SDS, 1 M NaCl), then polynucleotide kinase (PNK) buffer (50 mM Tris-HCl (pH 7.5), 10 mM MgCl₂, 0.5% NP-40).

Ligation of RNA ends

RNA 5'-ends were phosphorylated using 4 µl T4 PNK (NEB, catalog no. M0201) in a solution consisting of 8 µl 10x PNK buffer, 2 µl RNasin Plus (Promega, catalog no. N2615), 0.8 µl 100 mM ATP (ThermoFisher Scientific, catalog no. R0041), and 65.2 µl ddH₂O. Bead complexes were incubated for 40 minutes at 10°C then washed 3 times in PNK buffer. RNAs were then ligated by rotating for 16 hours at 4°C in 500 µl of RNA ligation solution (50 µl 10x T4 RNA ligase buffer, 60 µl 50% polyethylene glycol 8000, 125 µl 4M KCl, 12.5 µl RNasin Plus, 5 µl 100 mM ATP, 321.25 µl ddH₂O, and 50 µl T4 RNA ligase 1 (NEB, catalog no. M0204)). Bead complexes were then washed 3 times with 1 mL PNK buffer. Next, 80 µl of dephosphorylation solution (8 µl 10x dephosphorylation buffer, 2 µl RNasin Plus, 67 µl ddH₂O, and 3 µl alkaline phosphatase (Roche, catalog no. 10713023001)) was added to the beads, and RNA dephosphorylation was achieved by incubating samples for 40 minutes at 10°C, with intermittent 1,000 rpm shaking every 2 minutes for 15 seconds. The bead complexes were washed 2 times with 1 mL EGTA buffer (50 mM Tris-HCl (pH 7.5), 20 mM EGTA, 0.5% NP-40), and then three times with 1 mL PNK buffer.

Ligation of 3'-adapter

To ligate the miRCat-33 3'-linker (5'-TGGAATTCTCGGGTGCCAAGG-3') to the newly formed RNA hybrids, beads were incubated with 42 µl ddH₂O, 8 µl 10x T4 RNA ligase buffer, 16 µl 50% PEG-8000, 2 µl RNasin Plus, 8 pM of linker, and 4 µl T4 RNA ligase 2 (NEB, catalog no. M0239) for 16 hours at 16°C, with 1,000 rpm shaking every 2 minutes for 15 seconds. Bead complexes were then washed 3 times in PNK buffer.

Elution and RNA extraction

Bead complexes were incubated in 100 μ l of elution buffer (100 mM NaHCO₃, 1% SDS) for 15 minutes at 25°C on a 1,400 rpm shaker. After spinning at 1,000g for 1 minute, the elution buffer was transferred to a new tube. An additional 100 μ l of elution buffer was added to the bead complexes, elution was repeated and the eluates were then combined. To improve RNA phase separation of crosslinked RNA-AGO complexes, proteins were digested using proteinase K. 10 μ l of proteinase K (Roche, catalog no. 03115887001) in 40 μ l of proteinase K buffer (100 mM Tris-HCl (pH 7.5), 50 mM NaCl, 10 mM EDTA) was added to the 200 μ l of eluate and samples were incubated at 37°C for 20 min. Samples were then subjected to phenol-chloroform extraction to purify the RNA.

CLASH library preparation

RNA ends were phosphorylated, followed by ligation of the Solexa 5' linker (invddT-GTTCAR-GrArGrUrUrCrUrArCrArGrUrCrCrGrArCrGrArUrC-OH). RNA was re-extracted via phenol-chloroform, as described above. Sequencing libraries were prepared using the Illumina TruSeq Small RNA Sample Prep kit according to manufacturer's instructions, and cDNA was generated using SuperScript III reverse transcriptase (Invitrogen, catalog no. 18080093). The resulting samples were sequenced on an Illumina HiSeq 2500 machine.

RNA sequencing

RNA was extracted from Akata and SNU719 cells using TRIzol (ThermoFisher Scientific, catalog no. 15596026). Extraction was performed according to the manufacturer's instructions with one additional step included to improve the purity of the RNA: following isopropanol precipitation, RNA was reconstituted in 200 μ l ddH₂O with 20 μ l 3M sodium acetate and 500 μ l ethanol, stored at -20°C for 16 hours, spun down at 20,000 x g for 30 minutes at 4°C, and then resuming the manufacturer's protocol with the 70% ethanol wash step. Small fraction sequencing libraries were prepared using the Illumina TruSeq Small RNA Library Prep Kit (Illumina, catalog no. RS-200-0012), and poly-A sequencing libraries (HE2.1 and TIVE cells) were generated using the TruSeq RNA Sample Prep Kit (Illumina, catalog no. FC-122-1001).

Bioinformatic analysis

Adapter sequences were removed from raw sequencing reads using Trimmomatic². A transcriptome index was generated for *bowtie2*³ alignment, as previously described⁴, with the following modifications: a. GRCh38 transcript sequences were used (obtained from Gencode⁵; version 33), b. Annotated viral transcripts⁶ and miRNA sequences (obtained from mirBase⁷) were included in the index. Processed reads were aligned to the human and viral transcriptome indexes using *bowtie2* v2.3.3; alignments run with the following parameters: -D 20 -R 3 -N 0 -L 16 -k 20 -local -i S,1,0.50 -score-min L,18,0 -ma 1 -np 0 -mp 2,2 -rdg 5,1 -rfg 5,1). Hybrid alignments were retrieved from aligned reads using the *hyb* pipeline⁸ (<https://github.com/gkudla/hyb>). The structure and binding energies of each hybrid was predicted using the *RNAfold* algorithm of the *Vienna RNA* package⁹.

Targeting efficacy

Targeting efficacy for each miRNA-mRNA hybrid was calculated using the following equation:

$$t_{(microRNA_x, mRNA_y)} = \frac{microRNA_x: mRNA_y (h.c.p.m.)}{microRNA_x(c.p.m.) \times mRNA_y (t.p.m.)}$$

$$\begin{aligned} \text{miRNA} : \text{mRNA hybrid counts per million (h.c.p.m.)} \\ = 10^6 \times \left(\frac{\text{microRNA}_x : \text{mRNA}_y \text{ counts}}{\sum \text{microRNA}_n : \text{mRNA}_n \text{ counts}} \right) \end{aligned}$$

Hybrid counts were obtained via CLASH, mRNA t.p.m. were obtained from RNA-sequencing, and miRNA c.p.m. levels were quantified via small fraction sequencing.

AGO RNA immunoprecipitation

Approximately 5×10^6 SNU719 cells per reaction were lysed for 15 minutes on ice in 1 mL NP40 buffer (150 mM NaCl, 50mM Tris-HCl pH 8.0, 1% NP40 (Millipore Sigma, catalog no. 56741)) with 20uL of RNaseOUT (ThermoFisher Scientific, catalog no. 10777-019) and 10 uL of Protease Inhibitor Cocktail (Cell Signaling, catalog no. 5871). Lysates were spun at 20,000g for 15 minutes at 4C. Supernatants were transferred to a new tube. For each reaction, 30uL of Protein G magnetic beads (New England Biotechnology, catalog no. S1430S) were washed 3 times in 0.1M sodium phosphate and split into two tubes (one for preclearing lysates, the other for the pulldown of antibody-antigen complexes). For preclearing, the equivalent of 15uL of beads were added to lysates and rotated at 4C for 30 minutes. Tubes were put on a magnetic column and supernatants were transferred to a new tube. Either Mouse anti-pan Ago clone 2A8 (1:100 dilution; EMD Millipore, catalog no MABE56) or mouse anti-HA (1:50 dilution; Santa Cruz Biotechnology, catalog no. sc-7392) antibodies were added to precleared lysates and the tubes were rotated for 2h at 4C. The remaining Protein G beads were added, and tubes were rotated for 30m at 4C. Tubes were placed on a magnetic rack and supernatants were discarded. Beads were washed 3x with NP40 buffer then reconstituted in 150 uL of TE buffer (10mM Tris-HCl pH 8.0, 1 mM EDTA). 3 uL of proteinase K was added to each tube and tubes were incubated at 55C for 30 minutes. RNA was isolated via Phenol-Chloroform extraction followed by ethanol precipitation.

microRNA RT-qPCR

microRNA quantification was performed using a two-tailed RT-PCR approach[49]. RNA was reverse transcribed using M-MLV reverse transcriptase (Millipore Sigma, catalog no. M1302) according to the manufacturer's protocol, using pooled microRNA-specific RT primers at a final concentration of 1nM (see [S8 Table](#) for primer sets). qPCR using 1 μ L of the resulting cDNA was performed using iQ SYBR green Supermix (Bio-Rad, catalog no. 170-8882) on a Bio-Rad CFX96 instrument using the primers listed in [S8 Table](#). Amplification began with an initial denaturation step at 95°C for 3 minutes, followed by 40 cycles of 15 second denaturation at 95°C and 1 minute of annealing and extension at 53–60°C, depending on the predicted melting temperature of each primer set.

Principal component analysis

BL gene expression counts were transformed using the *normTransform* function of the *DESeq2* R package[50]. GC gene expression counts were transformed using the *vsd* function of the *vsn* R package[51]. Transformed counts were ranked by variance, and PCA was applied to the top 500 most variable genes in each tumor type using the *plotPCA* function of *DESeq2*. Each of the resulting principal components were compared to each relevant clinical covariate via logistic regression. *Pseudo-R²* values[52] were calculated for each principal component and covariate pair using the *PseudoR2* of the *descTools* R package.

Pathway analysis

CLASH derived mRNA targets for each virus and corresponding host were ranked by targeting efficacy in each cell line. Protein-protein interaction (PPI) and expression correlation networks were assembled for each of the top 20 targets using STRING[53] with default parameters, limited to 20 direct and 10 additional node proteins per queried “seed” gene. The resulting genes were explored for pathway enrichment with the *enrichR*[54] API, interrogating the Reactome library of pathways. Pathway enrichment was considered significant if the adjusted P-value < 0.05. All significant pathways were assigned to each seed gene.

Results

High expression of viral miRNAs in EBV-associated tumors

BLs and GCs are aggressive tumors with distinct etiologies. Pediatric BL is a B-cell malignancy endemic to sub-Saharan Africa that is characterized by the t(8;14)(q24;q32) *MYC:IGH* translocation[55,56]. GCs encompass a diverse group of epithelial tumors[57] originating from the stomach lining that have a broader epidemiology[58]. Despite overt differences in pathology and etiology, nearly all endemic BLs (over 90%)[47] and a subset of GCs (~10%)[6] are causally infected with EBV. As a first assessment of the viral contributions to these tumors, we performed principal component analysis (PCA) of 86 BL[47] (70 EBV+) and 235 GC[59] (24 EBV+) cell transcriptomes. Applying logistic regression to each of the top 10 (BL) or 15 (GC) principal components revealed that EBV status is a major distinguishing clinical covariate in both tumor types (Figs 1A and S1), indicating that EBV is likely a key determinant in shaping the tumor transcriptome.

To investigate underlying features of EBV that contribute to the tumor phenotype, we first carried out a quantitative assessment of the viral transcriptomes in EBV-associated BLs and GCs to identify candidate viral effectors in the natural tumor setting. Unlike lytic conditions, where 20% of expressed poly-adenylated RNAs in the cell are of viral origin (S2 Fig), the sum of expressed latency transcripts in BLs and GCs does not exceed 0.02% of cellular RNAs (Figs 1B and S3), with the majority of these being non-coding. Further, some of the EBV transcript signal in this analysis is derived from lytic gene expression occurring in a minor population of tumor cells through occasional sporadic reactivation. Therefore, long RNA latency viral gene expression represents only a minor portion of the overall transcriptome in these datasets. We were unable to assess expression of the highly abundant non-polyadenylated small non-coding viral EBER1 and EBER 2 transcripts because the GC dataset was polyA-selected and because they are partially lost following RNA size selection in the ribodepletion-derived BL dataset (which results in unreliable quantifications across samples).

Housed within the most abundantly expressed viral polyadenylated RNA, the long non-coding RNA (lncRNA), RPMS1, are 20 densely clustered intronic pre-miRNAs encoding at least 31 mature miRNAs (Figs 1C, S4, and S5). In contrast to the limited contribution of viral long RNAs to the tumor transcriptomes, the cumulative expression of viral miRNAs is remarkably high, exceeding host totals by as much as 3-fold (Fig 1D). This is particularly relevant because miRNA function is critically dependent on sufficient miRNA expression to saturate a high fraction of each target transcript. The importance of miRNA expression levels on function is supported by previous studies that showed that poorly expressed miRNAs have little discernable biological activity[60] whereas sufficient expression of an individual miRNA can have a marked impact on tumor biology[61]. The overwhelming expression of 31 viral miRNAs (Fig 1D and S1 Table) in EBV-positive BLs and GCs supports their likely relevance in modulating the tumor transcriptome landscape.

EBV miRNAs are over-represented in mRNA-bound RNA-induced silencing complexes (RISCs)

With the dependence on miRNA loading into RISC for target destabilization, the level of miRNA-RISC association is a predictor of miRNA targeting[62]. To assess RISC association characteristics of EBV and host miRNAs, we performed a modified version[42] of Crosslinking, Ligation, And Sequencing of Hybrids (CLASH)[63], referred to as qCLASH[42], in EBV+ cell lines modeling BL (Akata) and GC (SNU719) (S6A Fig). In CLASH, each AGO-bound miRNA-mRNA pair is ligated and then sequenced as a contiguous read, reproducibly resolving both the diversity of miRNA targets as well as the relative abundance of each interaction (S6B Fig).

In conjunction with our qCLASH analyses, we also performed standard small RNA fraction sequencing to assess the underlying expression of each miRNA in these cell lines. Notably, viral miRNA expression in Akata and SNU719 cell lines was substantially lower than the levels observed in primary tumors (Figs 2A and 2B, left, and S7). Nevertheless, this finding is in-line with previous studies showing that EBV miRNA levels are low in cell lines (including SNU719 cells) but increase markedly upon passage in immunocompromised mice[64,65], likely due to an enhanced reliance on viral miRNAs in the *in vivo* setting. Despite the modest expression of viral miRNAs in *in vitro* cultured SNU719 and Akata cells, we found a remarkably high representation of EBV miRNA-mRNA hybrids (Fig 2A and 2B, left). This observed enrichment was not attributable to a limited number of individual viral miRNAs with unusually high binding efficiencies, but instead was a characteristic that was broadly attributable to the bulk of EBV miRNAs (Fig 2A and 2B, right). These results indicate that in addition to exhibiting high *in vivo* expression, EBV miRNAs evolved with feature(s) that enhance RISC formation, supporting the possibility of distinctly productive viral miRNA targeting.

To determine whether enhanced representation of viral miRNAs in RISC is a conserved feature of γ HVs, we supplemented data from our previously published KSHV[42] and MHV68[66] qCLASH studies with small RNA sequencing to similarly compare KSHV and MHV68 hybrid levels to their respective miRNA expression. Similar to our findings with *in vitro* EBV miRNA expression, KSHV miRNAs were found to be expressed at low levels in KSHV infected LTC-TIVE cells (S8A Fig). Like our observations with EBV miRNAs, KSHV miRNAs exhibited marked enrichment in RISCs that was distributed across a spectrum of KSHV miRNAs (S8A Fig). In contrast, an aggregate assessment of MHV68 miRNAs did not show over-representation within RISCs (S8B Fig). This lack of aggregate MHV68 miRNA enrichment in RISC, however, may be related to their non-canonical processing mechanisms [67]. Nevertheless, at the individual miRNA level, we found that the two most overrepresented miRNAs within RISC in the MHV68-infected cell line, HE2.1, were the MHV68 M1-2-3p and M1-6-5p miRNAs (S8B Fig, right), suggesting that at least some MHV68 miRNAs are overrepresented in RISC. Together, these findings show preferential loading of viral miRNAs into RISC across these three γ HVs, representing a possible common strategy to exert strong influences on infected cell transcriptomes.

EBV miRNAs have high targeting efficacies

The disproportionately high association of viral miRNAs with RISCs could result from intrinsic properties of viral miRNAs that enhance loading into RISC. Nevertheless, high expression of viral miRNA and/or their targets could also contribute to the detection of greater numbers of miRNA-target RISCs. To account for the impact of miRNA and mRNA abundance on the level of AGO-bound miRNA-mRNA hybrids[68], we used an affinity constant calculation (dividing normalized hybrid counts by the normalized number of miRNAs and mRNA target

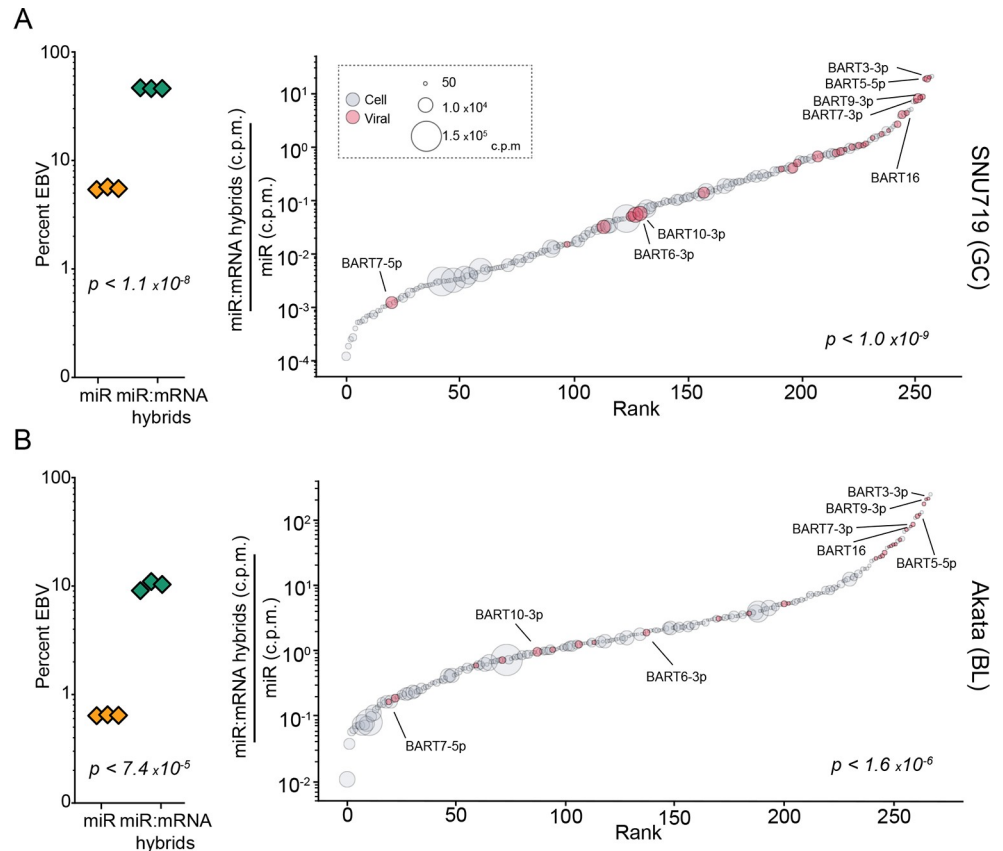


Fig 2. EBV miRNAs are over-represented in RNA induced silencing complexes (RISCs). CLASH and miRNA-sequencing were performed in triplicate for SNU719 and Akata cells. (A-B, left) The viral percentage of total miRNA expression in each sample, $\frac{\sum \text{viral microRNA (c.p.m.)}}{\sum \text{all microRNA (c.p.m.)}}$ (yellow triangles), and the percent of all miRNA-mRNA hybrids containing a viral miRNA, $\frac{\sum \text{viral miRNA:mRNA hybrids (h.c.p.m.)}}{\sum \text{all miRNA:mRNA hybrids (h.c.p.m.)}}$ (green triangles), were calculated. The indicated P-values were calculated using unpaired Student’s t-tests. (A-B, right) The average number of miRNA-mRNA hybrids formed for each miRNA was normalized to its baseline expression level, $\frac{\text{miRNA}_x\text{:mRNA hybrids (h.c.p.m.)}}{\text{miRNA}_x \text{ (c.p.m.)}}$. These mRNA-bound proportions were plotted in order of rank on the corresponding x-axis. Each circle represents an individual miRNA; circle size represents expression level; red circles indicate viral miRNAs. The indicated P-values were calculated using the Kolmogorov–Smirnov test (KS), comparing viral and human miRNAs.

<https://doi.org/10.1371/journal.ppat.1009217.g002>

transcripts *Fig 3C*) as a quantitative metric for miRNA “targeting efficacy”. We first assessed how accurately this targeting efficacy metric reflects intrinsic properties of miRNAs rather than cell specific factors. Unlike cellular miRNAs, nearly all viral 3’-UTR miRNA targets identified in Akata cells were also detected in SNU719 cells (*Fig 3A*), with the higher overall viral miRNA expression in SNU719 accounting for the additional miRNA targets identified in this system. Despite the overlap of specific targets, the relative abundance of each viral miRNA-mRNA hybrid detected in both cell lines was poorly correlated (*Fig 3B*), likely due to the differences in mRNA and/or miRNA expression in SNU719 and Akata cells. In contrast, viral miRNA targeting efficacies were strongly correlated between cell lines (*Fig 3D*). This finding also extended to cell miRNAs using miRNA/target interactions found in both cell lines (*Fig 3D*). These data support our contention that this targeting efficacy metric is a quantitative measure of intrinsic properties of miRNAs and their target sites that influence RISC formation.

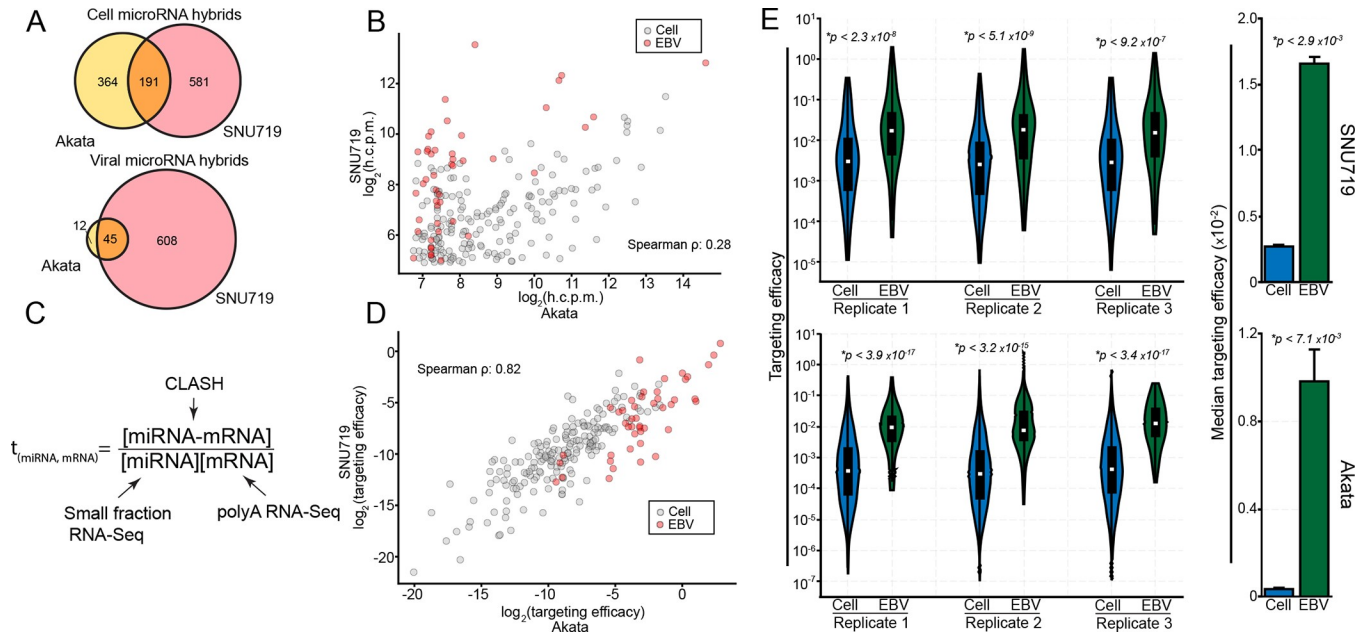


Fig 3. EBV miRNAs have high targeting efficacy. (A) Venn diagrams comparing genes found to be targeted in Akata and SNU719 cells by cellular (top) and viral (bottom) miRNAs. Only high confidence (>100 h.c.p.m. in Akata cells; >30 h.c.p.m. in SNU719 cells) 3'-UTR targets were considered. (B) h.c.p.m values for each interaction pair were compared between Akata and SNU719 cells, considering the high confidence interactions found in both cell lines. The \log_2 -transformed values from each cell line were correlated, resulting in a correlation coefficient of $\rho = 0.28$ (Spearman). (C) Schematic of the targeting efficacy calculation. (D) The \log_2 -transformed targeting efficacies were correlated between SNU719 and Akata cells, resulting in a spearman correlation coefficient of $\rho = 0.82$. (E; left) The distribution of targeting efficacies for each interaction in each CLASH replicate, comparing viral and cellular interactions. P-values were calculated using the KS test. (E; right) The median targeting efficacy of all three replicates. P-values were calculated using paired Student's t-tests.

<https://doi.org/10.1371/journal.ppat.1009217.g003>

We next applied targeting efficacy measures to assess the innate RISC loading properties of viral and cellular miRNAs in Akata and SNU719 cells. Across each biological replicate, the targeting efficacy distributions were substantially higher for EBV miRNAs than cell miRNAs in both SNU719 and Akata cells (Fig 3E and S2 Table). Extending this analysis to KSHV and MHV68 miRNAs, we similarly found that viral miRNAs have higher targeting efficacies than their cellular counterparts (S9A and S9B Fig and S2 Table). These results indicate that the higher proportion of viral miRNAs in RISCs relative to their expression levels is due to intrinsic properties of viral miRNAs that influence target selection and RISC loading. This suggests that viral miRNAs have evolved to be more effective inhibitors of their mRNA targets than host miRNAs.

EBV miRNAs target more accessible regions of mRNAs than cell miRNAs and form more thermodynamically stable hybrids

To assess biophysical properties underlying efficient viral miRNA RISC formation, we explored the nucleotide composition of miRNA/mRNA hybrids. Hybrid formation is guided in large part by the degree of complementarity between bases 2–8 of miRNAs and their targets, with loading into RISC being further boosted by the presence of an “A” opposite the first base of the miRNA[69]. These bases, collectively referred to as the “seed” region, display distinct complementarity patterns that are categorized into 9 different classes. With seed class being a known determinant of targeting effectiveness, we first tested whether there is a seed class bias for EBV miRNAs relative to cell miRNAs. As shown in S10 Fig, there is no discernable

enrichment of EBV miRNAs in seed classes with higher known targeting capabilities. Further, we found that within each seed class, viral miRNAs have higher targeting efficacies (Fig 4A). These data indicate that differential seed class utilization does not explain the increased targeting efficacy of EBV miRNAs.

In addition to the extent of seed matching, miRNA binding is improved when target sites are flanked by A/Us[70]. Considering the 4 bases directly adjacent to the seed binding site (2 bases on each side of the seed binding region), we found that for both cell and viral miRNAs, sites with high A/U content (3+ flanking A/Us) were associated with improved targeting efficacy (Figs 4B and S11A). Nevertheless, EBV, KSHV and MHV68 miRNAs tended to bind sites with fewer flanking A/Us (Figs 4C and S11B), indicating that the number of flanking A/Us fails to explain the higher targeting efficacies of viral miRNAs.

Because secondary structure at target sites reduces accessibility and interferes with RISC formation[71], transcript regions with less intramolecular binding tendencies are typically more effective miRNA targets. We therefore assessed target site accessibility for each CLASH hybrid using the RNAplfold[72] subpackage of the Vienna RNA suite using a window size and maximum base pairing separation of 80 and 40 bases, respectively. This analysis revealed that EBV miRNA target sites are, on average, more accessible than the target sites of host miRNAs (Fig 4D). This indicates that EBV miRNAs evolved to target more accessible regions, providing one likely explanation for the observed higher targeting efficacies of EBV miRNAs.

The last feature that we assessed to determine the molecular basis of enhanced EBV miRNA targeting efficacies was predicted minimum free energies of miRNA-mRNA hybrid pairs (across the entire miRNA and its target). This analysis revealed that EBV miRNA-mRNA hybrids tend to form more thermodynamically stable interactions than their cellular counterparts (Fig 4E). Extending this analysis to KSHV and MHV68 miRNAs, we found that like EBV miRNAs, KSHV and MHV68 miRNAs generally form more thermodynamically stable interactions than their cellular counterparts (S11C Fig). Together, these analyses indicate that γ HV miRNAs evolved with nucleotide sequence compositions that favor stronger hybrid interactions, providing another likely explanation for the enhanced targeting efficacy of viral miRNAs.

EBV miRNAs have a greater impact on their targets than their cellular miRNA counterparts

To test whether the higher overall targeting efficacies of EBV miRNAs translates to increased effectiveness in destabilizing their target mRNAs, we performed correlation analyses between the expression of each viral and cellular miRNA and their respective mRNA targets across EBV positive BL and GC datasets. Correlations were displayed in cumulative distribution plots (Fig 5). Shifts in distributions from permuted correlations of the same set of miRNAs with random mRNA targets were analyzed using the Kolmogorov-Smirnov (KS) test (Fig 5). In both BLs and GCs, viral miRNAs showed strong inverse correlations with their targets (BL, $p < 2.1 \times 10^{-6}$; GC, $p < 1.2 \times 10^{-5}$). In contrast, correlations between human miRNAs and their targets were less pronounced and not statistically significant. These results provide *in vivo* evidence of functional impacts of EBV miRNAs on targets identified by CLASH and they show that the higher targeting efficacies of EBV miRNAs likely translates into stronger functional influences on their targets.

EBV miRNA target distributions

In addition to assessing the impact that EBV miRNAs have on their individual targets, we also explored the breadth of viral miRNA targets to investigate the overall impact that EBV

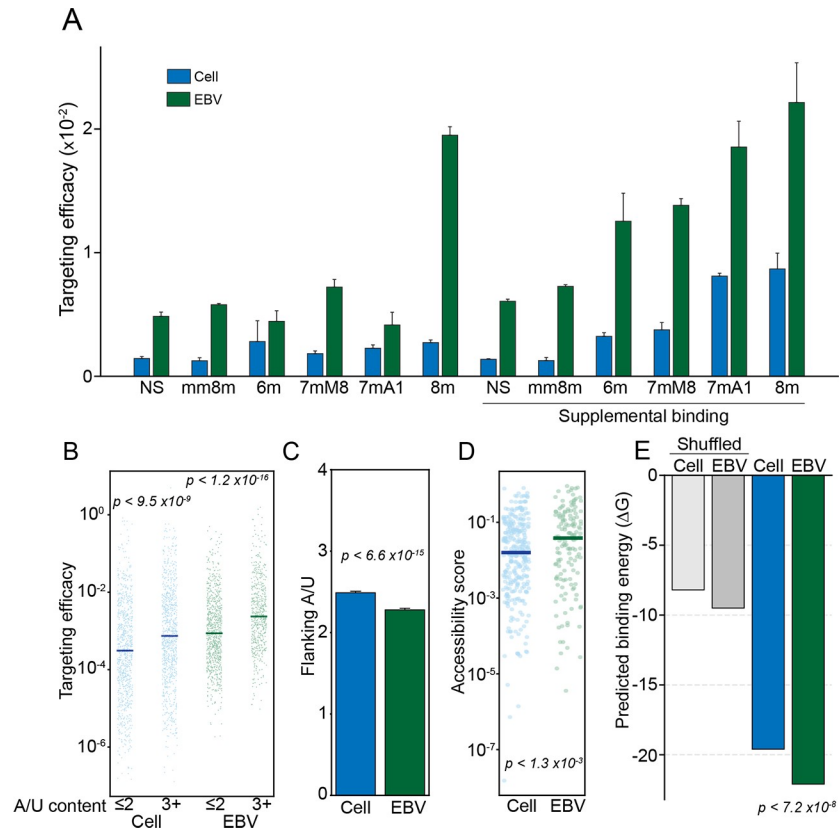


Fig 4. EBV miRNA hybrids are thermodynamically stable. Interactions in SNU719 cells were categorized by seed match type (NS, no seed; mm8m, mismatch 8mer; 6m, 6mer; 7mM8, 7mer base 8 match; 7mA1, 7mer A1 (A opposite base 1); 8m, 8mer), with “supplemental” interactions requiring >3 bases of complementarity between bases 13–17 of the miRNA and its target (similar results were obtained in Akata cells). (A) Median targeting efficacy for each type of seed match comparing viral and cellular miRNA interactions. (B) The targeting efficacy of each interaction binned by flanking A/U content of each miRNA target site. The two most proximal bases on each side of the seed binding region were considered. P-values were calculated using the KS test. (C) The mean number of flanking A/Us (max = 4) for cell and EBV miRNA target sites. P value was calculated via KS test. (D) The predicted local site accessibility score of each miRNA target site, using RNAplfold (using the following parameters: -W 80 -L 40 -u). The scores indicate the probability that all 14 bases, centered on position 7 of the miRNA target site, will be unpaired. P-values were calculated using the KS test. (E) Predicted minimum free binding energies (ΔG) were calculated for each hybrid using the RNAcofold function of the Vienna RNA Suite[107]. As a control, ΔG calculations were performed on shuffled sequences, with 100 permutations performed for each hybrid pair. The ΔG values of cellular and viral hybrids were compared by KS test.

<https://doi.org/10.1371/journal.ppat.1009217.g004>

miRNAs have on the cell transcriptome. We first quantified the number of targets attributable to each viral miRNA (Fig 6A). Several viral miRNAs predominantly target a single transcript (for example, BART3-3p:IPO7, BART17-3p:MED13, and BART20-5p:UBE2H), while others such as BART5-5p, BART7-3p, BART9-3p, and BART16 have many strong targets. The predicted seed-pairing stability (SPS; the predicted binding energy of positions 2–8 of a miRNA bound to its reverse complement target) of miRNAs has been previously shown to be a predictor of how promiscuous the miRNA is[73]. This finding appears to be borne out for EBV miRNAs. For example, BART7-3p (AUCAUAG; SPS $\Delta G^\circ = -5.53 \text{ kcal mol}^{-1}$), BART9-3p (AACACUU; SPS $\Delta G^\circ = -5.54 \text{ kcal mol}^{-1}$), and BART16 (UAGAUAG; SPS $\Delta G^\circ = -5.73 \text{ kcal mol}^{-1}$); have relatively low SPS values[73] (S3 Table) and extensively target a multitude of mRNAs (including hybrids with at least 100 h.c.p.m., BART7-3p has 128 distinct targets, BART16, 35, and BART9-3p, 25). BART5-5p (AAGGUGA; SPS $\Delta G^\circ = -7.98 \text{ kcal mol}^{-1}$) has an

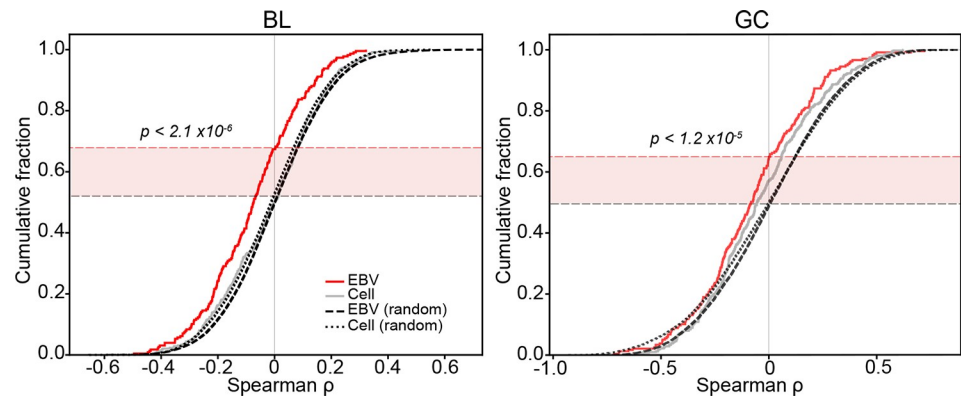


Fig 5. EBV miRNAs and their targets have strong inverse correlations in primary BLs and GCs. For each CLASH miRNA-mRNA hybrid, mRNA and miRNA expression levels (c.p.m.) were correlated across all EBV-positive BL and GC tumors. Correlations were performed on hybrids that met the following criteria: 1. Average miRNA expression in tumors ≥ 10 c.p.m., 2. Average mRNA expression in tumors > 5 t.p.m., 3. $\frac{h.c.p.m.}{mRNA\ t.p.m.} > 3$, and 4. miRNA-mRNA interactions occurred within the 3'-UTR, where miRNA mediated repression is more often effective [108]. Cumulative distribution plots were generated using ranked Spearman correlation coefficients for each species. As a control, expression levels of the miRNA of each hybrid pair analyzed was correlated with expression levels of a random mRNA across the same tumors. For each randomized interaction, 100 permutations were run. Correlation values of EBV miRNA-mRNA pairs were compared to randomized controls; P-values were generated using the KS test.

<https://doi.org/10.1371/journal.ppat.1009217.g005>

average SPS (ranking in the 48th percentile of all cellular miRNAs) with an intermediate number (82) of high abundance targets. MiRNAs with high SPS, such as BART3-3p (GCACCAC; SPS $\Delta G^\circ = -11.29$ kcal mol⁻¹), BART17-3p (GUAUGCC; SPS $\Delta G^\circ = -9.37$ kcal mol⁻¹), and BART20-5p (AGCAGGC; SPS $\Delta G^\circ = -11.53$ kcal mol⁻¹), which have 11, 4, and 1 high abundance target(s), respectively. These high SPS miRNAs tend to extensively target one transcript, with BART3-3p targeting IPO7 over 12-fold more often than its next most frequent interaction partner, BART17-3p:RBM8A accounting for nearly 8-fold more hybrids than its next best target, and BART20-5p:UBE2H representing over 2-fold more hybrids than its next most common target. Overall, despite the relatively focused functions of some EBV miRNAs, EBV miRNAs as a whole tend to display greater breadth in targets than their cellular counterparts (Fig 6B). This may be a means through which EBV evolved to influence a larger target set despite having a smaller repertoire of encoded miRNAs.

While EBV miRNA targeting is generally spread across more transcripts, they tend to be directed towards transcripts regulated by fewer miRNAs (Fig 6C). This indicates that cellular miRNAs more often work in a cooperative fashion. The higher targeting efficacies of viral miRNAs may reduce their requirement for cooperative targeting, as they tend to target a repertoire of transcripts that are distinct from cellular miRNAs. As an extension of their enhanced targeting efficacy, viral miRNAs are not constrained by the necessity of cooperative targeting, allowing them each to serve a unique purpose, and increasing their influence over host cell transcriptomes.

EBV miRNAs interfere with immune signaling in the tumor microenvironment

Next, we sought to investigate the potential functional impact of the most influential EBV miRNA-target interactions in modulating the host cell environment. Using the targets of the top 20 EBV miRNA-target interactions as network seed genes, we applied enrichR [54] to query pathway enrichment for each seed gene and its 20 strongest interacting partners. As a control, we performed a similar analysis on the targets of the top 20 cell miRNA-target

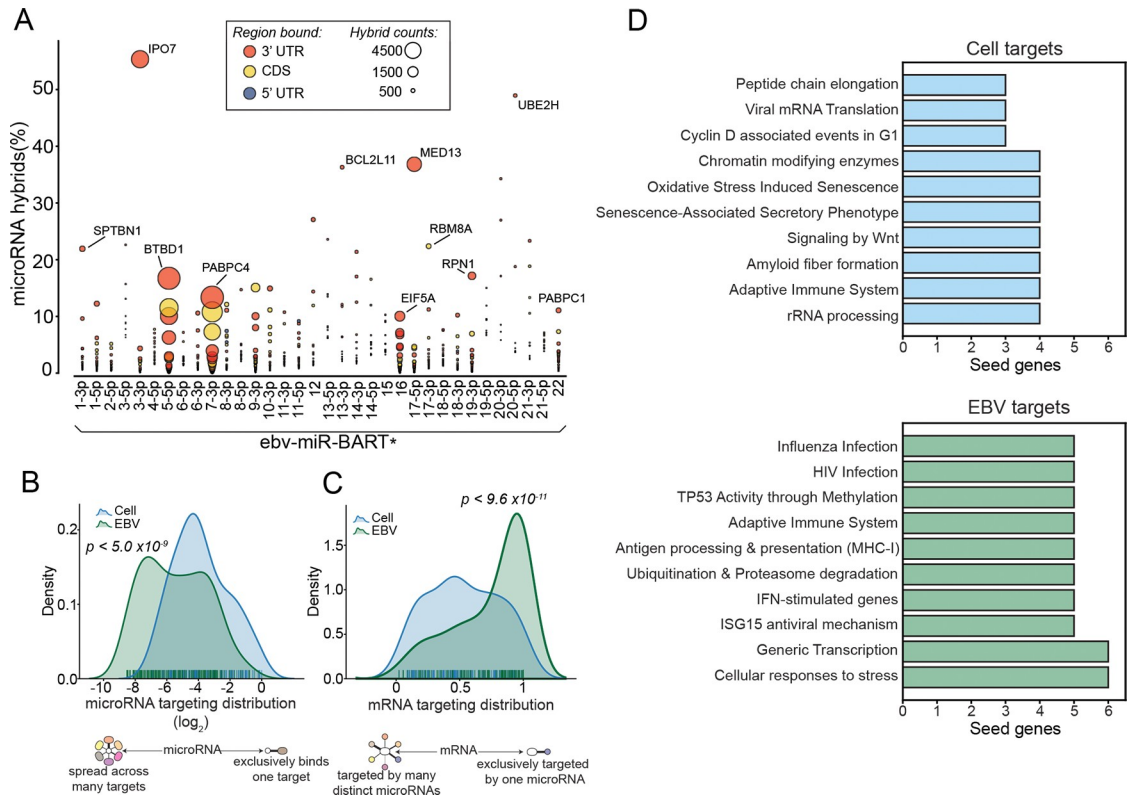


Fig 6. γ HV miRNAs target components of immune signaling pathways. (A) SNU719 hybrids containing EBV miRNAs. Each interaction was represented by a circle; circle size corresponds to the total number of hybrids formed ($microRNA_x : mRNA_y$, *h.c.p.m.*); The y-axis values represent the percent of all hybrids that contain the indicated miRNA, $\frac{microRNA_x:mRNA_y}{\sum microRNA_x:mRNA_y}$, *h.c.p.m.*. (B) The distribution of y-axis values from (A), extended to all hybrids. Cellular and viral hybrids were compared; P-value was generated using the KS test. (C) The fraction of individual miRNAs hybridizing with each mRNA, $\frac{microRNA_x:mRNA_y}{\sum microRNA_x:mRNA_y}$, *h.c.p.m.*, comparing viral and human distributions; P-value was generated using the KS test. (D) Pathways targeted by EBV and cellular miRNAs. Protein-protein interaction networks of each of the top 20 EBV or cellular target genes were obtained from StringDB[53], and resulting protein names were submitted to Enrichr[54] for pathway enrichment analysis (interrogating pathways included in the Reactome database). All statistically significant pathways (FDR < 0.05) were assigned to the target gene.

<https://doi.org/10.1371/journal.ppat.1009217.g006>

interactions. This analysis revealed selective enrichment for Influenza and HIV infection, antigen processing and presentation (MHC class I), Ubiquitin & Proteasome degradation (which can impact antigen processing and presentation) and IFN-stimulated genes and ISG15 antiviral mechanisms as top EBV miRNA pathway hits (Fig 6D and S4 Table). This suggests that the EBV miRNA-target interactions within the top 20 highest targeting efficacy interface with adaptive and innate immune response pathways.

Previous studies have shown that EBV positive GCs have higher immune cell infiltration than their EBV negative counterparts[74], likely due to sporadic expression of lytic viral proteins within the tumor. Consistent with these studies, we used CIBERSORTx[75] to infer the immune cell infiltration in each tumor through deconvolution of immune cell signatures within the GC dataset (using only the microsatellite stable (MSS)-only cohort) and found higher levels of T-cell and macrophage subtypes in the EBV positive cohorts (S12A Fig). We also determined the diversity of infiltrating T-cells within these tumors by assessing the number of unique T-cell receptor sequences for each tumor. Utilizing MIXCR[76], we realigned each tumor RNA-seq dataset to all potential combinations of rearranged T-cell receptors and used VDJTOOLS[77] for QC and T-cell clone quantifications. This analysis showed that

consistent with the finding of higher levels of T-cell infiltration in EBV positive GCs through CIBERSORTx analysis, we found a greater diversity of T-cell clones in EBV positive tumors than in EBV negative tumors (S12B Fig). Together, these results confirm the findings of The Cancer Genome Atlas Research Network[57], showing that EBV likely induces some level of adaptive immune response in EBV positive GCs.

While the presence of EBV clearly induces immune cell infiltration into EBV associated tumors, we hypothesized that the interactions of viral miRNAs with immune regulatory pathways in infected cells acts as a counter measure to mitigate immune cell-mediated targeting of virus-infected tumor cells. To functionally assess this possibility we first identified potential direct and indirect targets of viral miRNAs in the EBV+ BL and GC cohorts by correlating the sum of viral miRNA expression values with the expression levels of each cell gene (S5 Table). Gene Set Enrichment Analysis (GSEA)[78,79], using the pre-ranked BL and GC miRNA-gene correlations, revealed that viral miRNA expression negatively correlates with the IFN γ and TNF α signaling pathways (Fig 7A). The inverse relationship between IFN γ and TNF α signaling pathways and EBV miRNA expression suggests that EBV miRNAs mitigate IFN γ - and TNF α - mediated amplification of the immune response. To more directly assess the relationship between EBV miRNAs and adaptive immune response, we used CIBERSORTx[75] to infer immune cell infiltration in each tumor sample from the BL and GC datasets (S6 Table). This analysis showed that CD8 T-cells, CD4 T-cells, and macrophages inversely correlate with viral miRNA expression (Fig 7B). Assessing the infiltrating T-cell diversity across these tumors showed a strong inverse correlation between unique T-cell clonotype counts and viral miRNA expression (Fig 7C and S7 Table), further supporting a role of EBV miRNAs in interfering with the immune response to EBV infection within these tumors. These findings are most tightly associated with EBV miRNAs rather than other expressed EBV transcripts since EBV miRNAs show a stronger inverse relationship with T-cell clonotype numbers than viral pol II transcripts (S13 Fig). Together these analyses provide evidence that the targeting of components of immune response pathways by EBV miRNAs results in the dampening of innate and adaptive immune responses to viral infection in EBV positive cancers.

Discussion

By integrating miRNA and mRNA expression levels with hybrid quantifications obtained via CLASH, we used an affinity constant calculation to assess targeting efficacy for each interaction. Comparing targeting efficacies of viral and host miRNA-target interactions, we found that viral miRNAs generally bind their targets more effectively than host miRNAs. The elevated efficacy of EBV miRNA-mRNA interactions transcended seed match and the level of flanking AU content. Instead, we found that the complexes formed between EBV miRNAs and their targets were more thermodynamically stable and tended to occur at target sites with less secondary structure. In metazoans, broadly conserved miRNA target sites tend to facilitate the most effective targeting interactions. However, these sites exhibit a negative selection over time that tempers miRNA binding efficacy. Unlike targets of broadly expressed miRNAs, co-expressed targets of miRNAs that exhibit tissue specific expression tend to evolve effectivity-reducing alterations in target sites[80], suggesting that the major role of miRNAs is to fine-tune gene expression rather than to significantly alter it[81]. The continued coevolution of cell miRNAs and their target genes presents an internal arms race that ultimately reduces the impact of the majority of miRNA-mRNA interactions. These constraints do not apply to viral miRNAs which have evolved to effectively target a large number of host transcripts, with some miRNAs such as BART7-3p effectively binding many target mRNAs, and others, such as BART3-3p, homing in on a single transcript (notably, this latter class of viral miRNA might

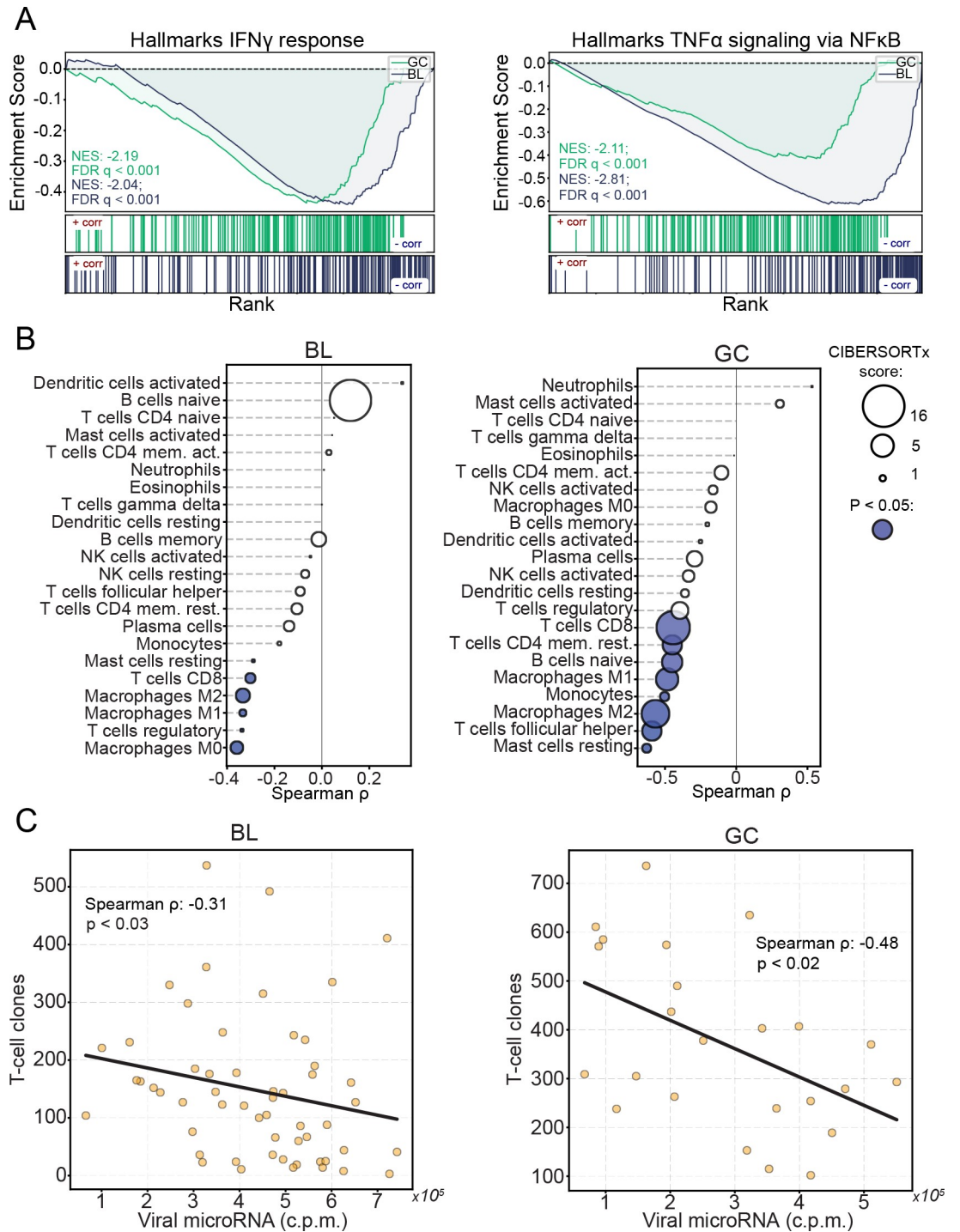


Fig 7. Viral miRNAs interfere with anti-viral immunity. The sum of all viral miRNA c.p.m. was correlated to expression levels of each mRNA (c.p.m.) in EBV-positive BL and GC tumors. The correlations were ranked, then gene lists were interrogated using GSEA. (A) Stacked GSEA curves of the Hallmarks IFN γ signaling pathway (left) and the TNF α -NF κ B signaling pathway (right). NES, nominal enrichment score, FDR, false discovery rate. (B) Immune cell infiltrates were inferred using CIBERSORTx. Each cell type was correlated (spearman) to the sum of EBV miRNAs across EBV-positive BLs and GCs. Circle size represents the average CIBERSORTx absolute score across all tumors, filled circles represent statistically significant (P < 0.05) spearman correlations. (C) T-cell clonotypes were obtained for each EBV-positive tumor sample using MIXCR; The number of unique clonotypes was correlated with the sum of viral miRNAs in EBV-positive BLs and GCs.

<https://doi.org/10.1371/journal.ppat.1009217.g007>

implicate singular targets that are critical to viral persistence and/or expansion in host cells, potentially presenting a vulnerability to the virus). The tendency of viral miRNAs to exhibit high targeting efficacies therefore arm them with the unmatched ability to influence the landscape of host RNA expression.

A longstanding challenge in deciphering miRNA function is the accurate assessment of its targets[82]. Because the most favorable interactions require only 7 bases of complementarity, even the most infrequent 3' UTR binding motifs are widely dispersed throughout the transcriptome. Still, the number of true miRNA binding sites is at least an order of magnitude lower than the number of seed complementary sequences in transcriptome 3' UTRs. The ability to discern true miRNA targets has improved dramatically with the advent and continued development of binding site prediction algorithms[70,82], and even more so with high throughput experimental approaches such as PAR-CLIP[83]. These tools have seeded studies of EBV miRNA functions, leading to the discovery of consequential mRNA targets[84] including mediators of apoptotic signaling, BBC3 (BART5-5p)[85] and BAD (BART20-5p)[86] and regulators of innate immunity, NDRG1 (multiple)[87], MICB (BART2-5p)[88], IFI30 (BART1 and BART2), LGMN (BART1 and BART2), and CTSB (BART1 and BART2)[89]. However, both putative and empirically identified viral miRNA targets have often been difficult to validate[90]. In our system, the BBC3 interaction was the 220th most prevalent hybrid of BART5-5p (38 h.c.p.m.), CTSB was the 375th most abundant BART1-5p target (6 h.c.p.m.), and combined, NDRG1 hybrids ranked 3681st among all viral miRNA targets (25 h.c.p.m.). We were unable to detect any viral miRNA hybrids with IFI30, LGMN, or BAD, while MICB and IL12A were not sufficiently expressed in SNU719 cells. Overall, little overlap exists between targets identified among previously published high throughput EBV miRNA targetome studies[90], yet one consistently identified interaction is that between BART3-3p and IPO7, an interaction that has subsequently been used as a control in studies of EBV miRNA targeting[35,91]. In our study, we detect substantial levels of this interaction (6846 h.c.p.m.; ranked 1st among BART3-3p targets), suggesting that the quantitative nature of this approach helps distinguish the targets of both viral and host miRNAs that are likely to be impacted the most.

Among the most frequent targets of several EBV miRNAs were transcripts coding for ubiquitin ligases and adapters. These include the E3 ubiquitin ligases, FBXO21 (BART21-5p; ranked 1st among all BART21-5p interactions), TRIM65 (BART7-3p; ranked 5th), RNF38 (BART5-5p; ranked 7th), TRIM8 (BART16; ranked 1st), and KCMF1 (BART1-3p; ranked 2nd and BART3-3p; ranked 2nd), the E2 ubiquitin ligase, UBE2H (BART20-5p; ranked 1st and BART7-3p; ranked 17th), and the E3 ubiquitin ligase adapters, BTBD1 (BART5-5p; ranked 1st) and UBXN7 (BART5-5p; ranked 16th). Several of these ubiquitin ligases have important roles in host intrinsic immunity against viral infection. Both FBXO21 and TRIM65 are necessary for the production of type I IFNs in response to viral infection[92,93]. TRIM8 is a potent activator of TNF α and NF κ B signaling[94], both pathways of which we found to have a strong inverse correlation with viral miRNAs in BLs and GCs (Fig 7A).

A more general possible functional consequence of inhibiting ubiquitin ligase expression is interference with MHC class I antigen presentation. Previous studies have shown that EBV miRNAs collectively reduce host cell antigen presentation, culminating in the subversion of CD4+ and CD8+ T-cell surveillance[89,95,96]. Numerous viruses have evolved various mechanisms to interfere with this pathway. For example, the HIV NEF protein redirects HLA-A and HLA-B transportation[97], the Hepatitis B Virus X protein interferes with proteasomal activity[98], K3 and K5 of KSHV promote MHC-I endocytosis and destruction[99], MHV68 MK3 is a ubiquitin ligase that targets MHC-I for destruction[100], and both the U6 protein of HCMV and EBV encoded BNLF2A inhibit TAP-mediated peptide transport and subsequent MHC loading[101–103]. While viral protein expression is restricted in EBV-associated

tumors, the presence of the virus still elicits an immune response and mutations that help drive tumors produce neo-epitopes that immune cells may recognize as foreign. The survival of EBV positive cells, including tumors, therefore, requires immune subversion or escape [104]. Previous studies have shown that EBV miRNA expression is elevated by inoculation of tissue culture grown EBV positive tumor cells in mice [105]. Furthermore, we found that EBV miRNAs inversely correlate with immune cell infiltrates in BLs and GCs, suggesting that an important role of the viral miRNAs is to interfere with immune surveillance, thereby helping facilitate the survival and expansion of the underlying tumor.

Altogether, our findings show that EBV miRNAs are uniquely effective inhibitors of target RNAs through facilitating high *in vivo* expression and the targeting of accessible sites with more favorable miRNA/target binding energies, thereby achieving conserved impacts on immune responses to infected tumor cell populations.

Supporting information

S1 Fig. EBV status is the most impactful clinical covariate in BLs and GCs. Variance stabilized BL and GC RNA expression values were subjected to principal component analysis (PCA). Logistic regression was performed comparing each of the first ten (BL) or fifteen (GC) principal components with the indicated clinical covariate [47,48,57]. The resulting R^2 values from were plotted as a heatmap. (A) The BL analysis was restricted to tumors passing QC (the “Discovery” cohort) [47] (left), EBV-positive tumors of the “Discovery” cohort (center), and the EBV-positive, fresh, frozen tumors from the “Discovery” cohort (right). (B) The GC analysis included all tumors (left), exclusively microsatellite stable (MSS) tumors (center), and only MSS and EBV-positive GCs (right).

(TIF)

S2 Fig. Substantial EBV gene expression during lytic reactivation is restricted in latency.

Raw sequencing reads of latent and Zta-induced Akata cells (SRA accession: SRP042043) [109] were aligned to the combined hg38 + EBV reference transcriptome using kallisto [46]. The viral percentage of expressed mRNAs was calculated using the following equation,

$$\frac{\sum \text{viral transcripts (t.p.m.)}}{10^6}$$

Viral non-coding transcripts are in gray; viral coding transcripts are in orange.

(TIF)

S3 Fig. The EBV gene expression pattern in EBV-positive BLs and GCs. A heatmap of viral gene expression (t.p.m.) in BL and GC tumors. The heatmap does not include EBER1 or EBER2 (their sizes, 167 and 172 nucleotides, are slightly below the purified fragment size used to generate the RNA-seq libraries). RNA-sequencing of GC tumors was not strand specific and lytic genes that overlap RPMS1 and/or A73 are marked with “*” since these values likely represent misattributed RPMS1 or A73 expression.

(TIF)

S4 Fig. EBV microRNA expression in EBV-positive BLs and GCs. A heatmap of viral microRNA expression (c.p.m.) across all BL and GC tumors. Reads were aligned to the combined EBV and human mature microRNA references (miRBase v22) using bowtie2 [110].

(TIF)

S5 Fig. RPMS1 and EBV microRNAs are correlated in BLs and GCs. The sum of all viral microRNAs (c.p.m.) was correlated with RPMS1 expression (t.p.m.) in EBV-positive BL and GC tumors.

(TIF)

S6 Fig. CLASH overview and reproducibility. (A) Schematic of the CLASH protocol[41,42]. CLASH sequencing reads were processed using the *hyb* bioinformatic pipeline[111] and in house scripts (https://github.com/flemingtonlab/ebv_clash). (B) Normalized counts (hybrid counts per million, h.c.p.m.) of each microRNA-mRNA pair were correlated pairwise between replicate samples; pearson correlation coefficients are indicated.

(TIF)

S7 Fig. Comparison of loading efficiencies calculated from CLASH-RNA-seq or α -AGO IP-RT-qPCR. To validate the loading efficiency values obtained via CLASH and small fraction RNA-sequencing (see Fig 2), we performed an α -AGO immunoprecipitation without cross-linking or ligation, followed by qRT-PCR for several selected microRNAs. The loading efficiency for each microRNA was calculated by taking the Δ Ct between AGO-IP and input sample ($2^{-(\Delta\text{AgO}_{Ct} - \text{Input}_{Ct})}$; x-axis). These values were compared to those obtained using CLASH and small fraction RNA-seq ($\frac{\text{microRNA}_x:\text{mRNA (h.c.p.m.)}}{\text{microRNA}_x(\text{c.p.m.})}$; y-axis), resulting in a spearman correlation coefficient of $\rho = 0.64$.

(TIF)

S8 Fig. γ HV microRNAs are overrepresented within RISC. Raw CLASH sequencing reads were obtained for KSHV infected TIVE-EX-LTC[42] (SRA accessions:

SRR5876950-SRR5876952) and MHV68 infected HE2.1[66] (SRA accessions:

SRR8395245-SRR8395247) cell lines, with small fraction sequencing performed on the same cell lines. (A-B; left) Yellow triangles display total viral microRNA expression,

$\frac{\sum \text{viral microRNA (c.p.m.)}}{10^6}$; green triangles represent the percent of all microRNA-mRNA hybrids containing a viral microRNA, $\frac{\sum \text{viral microRNA:mRNA hybrids (h.c.p.m.)}}{10^6}$. P-values were calculated using unpaired Student's t-tests. (A-B; right) MicroRNA-mRNA hybrid abundance was normalized to baseline expression for each individual microRNA, $\frac{\text{microRNA}_x:\text{mRNA (h.c.p.m.)}}{\text{microRNA}_x(\text{c.p.m.})}$ (see Fig 2). Viral and host microRNA ranks were compared; P-values were calculated using the Kolmogorov-Smirnov test (KS).

(TIF)

(TIF)

S9 Fig. γ HV microRNAs bind efficiently to their targets. (A-B; left panels) Hybridization efficacy values were tabulated (see Fig 3B) for each CLASH replicate, comparing viral and host interactions. P-values were calculated using the Kolmogorov-Smirnov test. (A-B; right panels) The mean hybridization efficacy of viral and host hybrids from all three replicates; P-values were calculated using paired Student's t-tests.

(TIF)

S10 Fig. Seed match of each microRNA-mRNA interaction. The number of unique interactions of each type of seed match were compared between viral and cellular microRNAs.

(TIF)

S11 Fig. γ HV microRNA-mRNA interactions are thermodynamically stable. (See Fig 4).

(A) The targeting efficacy of each interaction binned by flanking A/U content of each microRNA target site. P-values were calculated using the KS test. (B) The mean number of flanking A/Us (max = 4) for cellular and KSHV (top) or MHV68 (bottom) microRNA target sites. P value was calculated via KS test. (C) Predicted minimum free binding energies (Δ G) were calculated for each hybrid using the RNAfold function of the Vienna RNA Suite[107]. As a control, Δ G calculations were performed on shuffled sequences, with 100 permutations

performed for each hybrid pair. The ΔG values of cellular and viral hybrids were compared by KS test.

(TIF)

S12 Fig. Elevated immune cell infiltrates in EBV-positive GCs. (A) Immune cell abundances were inferred using CIBERSORTx. Tumor immune cell compositions were compared between EBV-positive and EBV-negative BL and GC tumors. Circle size represents the average CIBERSORTx absolute score across all tumors, filled circles represent statistically significant ($P < 0.05$) fold changes; P-values were calculated using Mann Whitney U tests. (B) The number of unique T-cell clonotypes was compared between EBV-positive and EBV-negative BL and GC tumors. P-values were calculated using unpaired Student's t-tests.

(TIF)

S13 Fig. Viral microRNAs have the strongest inverse correlation with T-cell diversity among viral transcripts. Expression values of each EBV lncRNA, mRNA, and microRNA was correlated with counts of unique T-cell clonotypes in EBV-positive BL and GC tumors. Spearman correlation coefficients were plotted in ranked order.

(TIF)

S1 Table. MicroRNA expression in clinical BL and GC samples.

(XLSX)

S2 Table. CLASH-derived microRNA targeting efficacies.

(XLSX)

S3 Table. Gammaherpesviral microRNA sequences (obtained from mirBase).

(XLSX)

S4 Table. Pathway network analysis of microRNA targets.

(XLSX)

S5 Table. Gene correlations with viral microRNAs in clinical BLs and GCs.

(XLSX)

S6 Table. CIBERSORT score correlations with EBV microRNAs in clinical BL and GC samples.

(XLSX)

S7 Table. T-cell receptor clonotypes detected in each BL and GC tumor.

(XLSX)

S8 Table. Primer sequences.

(XLSX)

Author Contributions

Conceptualization: Nathan Ungerleider, Rolf Renne, Scott Tibbetts, Erik K. Flemington.

Data curation: Nathan Ungerleider, Erik K. Flemington.

Formal analysis: Nathan Ungerleider, Erik K. Flemington.

Funding acquisition: Nathan Ungerleider, Erik K. Flemington.

Investigation: Whitney Bullard, Mehmet Kara, Xia Wang, Claire Roberts.

Methodology: Rolf Renne.

Visualization: Nathan Ungerleider.

Writing – original draft: Nathan Ungerleider, Erik K. Flemington.

Writing – review & editing: Nathan Ungerleider, Rolf Renne, Scott Tibbetts, Erik K. Flemington.

References

1. Epstein MA, Achong BG, Barr YM. Virus Particles in Cultured Lymphoblasts from Burkitt's Lymphoma. *Lancet*. 1964; 1(7335):702–3. [https://doi.org/10.1016/s0140-6736\(64\)91524-7](https://doi.org/10.1016/s0140-6736(64)91524-7) PMID: 14107961.
2. Xiong J, Cui BW, Wang N, Dai YT, Zhang H, Wang CF, et al. Genomic and Transcriptomic Characterization of Natural Killer T Cell Lymphoma. *Cancer Cell*. 2020; 37(3):403–19 e6. Epub 2020/03/19. <https://doi.org/10.1016/j.ccell.2020.02.005> PMID: 32183952.
3. Oyama T, Yamamoto K, Asano N, Oshiro A, Suzuki R, Kagami Y, et al. Age-related EBV-associated B-cell lymphoproliferative disorders constitute a distinct clinicopathologic group: a study of 96 patients. *Clin Cancer Res*. 2007; 13(17):5124–32. Epub 2007/09/06. <https://doi.org/10.1158/1078-0432.CCR-06-2823> PMID: 17785567.
4. Hjalgrim H, Askling J, Rostgaard K, Hamilton-Dutoit S, Frisch M, Zhang JS, et al. Characteristics of Hodgkin's lymphoma after infectious mononucleosis. *N Engl J Med*. 2003; 349(14):1324–32. Epub 2003/10/03. <https://doi.org/10.1056/NEJMoa023141> PMID: 14523140.
5. zur Hausen H, Schulte-Holthausen H, Klein G, Henle W, Henle G, Clifford P, et al. EBV DNA in biopsies of Burkitt tumours and anaplastic carcinomas of the nasopharynx. *Nature*. 1970; 228(5276):1056–8. <https://doi.org/10.1038/2281056a0> PMID: 4320657.
6. Shibata D, Weiss LM. Epstein-Barr virus-associated gastric adenocarcinoma. *Am J Pathol*. 1992; 140(4):769–74. Epub 1992/04/01. PMID: 1314023; PubMed Central PMCID: PMC1886378.
7. Messick TE, Smith GR, Soldan SS, McDonnell ME, Deakyne JS, Malecka KA, et al. Structure-based design of small-molecule inhibitors of EBNA1 DNA binding blocks Epstein-Barr virus latent infection and tumor growth. *Science Translational Medicine*. 2019; 11(482). ARTN eaau5612 <https://doi.org/10.1126/scitranslmed.aau5612> WOS:000460393700003. PMID: 30842315
8. Munz C. Latency and lytic replication in Epstein-Barr virus-associated oncogenesis. *Nat Rev Microbiol*. 2019; 17(11):691–700. Epub 2019/09/04. <https://doi.org/10.1038/s41579-019-0249-7> PMID: 31477887.
9. Chijioke O, Muller A, Feederle R, Barros MH, Krieg C, Emmel V, et al. Human natural killer cells prevent infectious mononucleosis features by targeting lytic Epstein-Barr virus infection. *Cell Rep*. 2013; 5(6):1489–98. Epub 2013/12/24. <https://doi.org/10.1016/j.celrep.2013.11.041> PMID: 24360958; PubMed Central PMCID: PMC3895765.
10. Henderson S, Rowe M, Gregory C, Croom-Carter D, Wang F, Longnecker R, et al. Induction of bcl-2 expression by Epstein-Barr virus latent membrane protein 1 protects infected B cells from programmed cell death. *Cell*. 1991; 65(7):1107–15. Epub 1991/06/28. [https://doi.org/10.1016/0092-8674\(91\)90007-I](https://doi.org/10.1016/0092-8674(91)90007-I) PMID: 1648447.
11. Kilger E, Kieser A, Baumann M, Hammerschmidt W. Epstein-Barr virus-mediated B-cell proliferation is dependent upon latent membrane protein 1, which simulates an activated CD40 receptor. *EMBO J*. 1998; 17(6):1700–9. Epub 1998/05/02. <https://doi.org/10.1093/emboj/17.6.1700> PMID: 9501091; PubMed Central PMCID: PMC1170517.
12. Yin Y, Manoury B, Fahraeus R. Self-inhibition of synthesis and antigen presentation by Epstein-Barr virus-encoded EBNA1. *Science*. 2003; 301(5638):1371–4. Epub 2003/09/06. <https://doi.org/10.1126/science.1088902> PMID: 12958359.
13. Kuppers R. B cells under influence: transformation of B cells by Epstein-Barr virus. *Nat Rev Immunol*. 2003; 3(10):801–12. Epub 2003/10/03. <https://doi.org/10.1038/nri1201> PMID: 14523386.
14. Raab-Traub N. Epstein-Barr virus in the pathogenesis of NPC. *Semin Cancer Biol*. 2002; 12(6):431–41. Epub 2002/11/27. <https://doi.org/10.1016/s1044579x0200086x> PMID: 12450729.
15. Kennedy G, Komano J, Sugden B. Epstein-Barr virus provides a survival factor to Burkitt's lymphomas. *Proceedings of the National Academy of Sciences*. 2003; 100(24):14269–74. <https://doi.org/10.1073/pnas.2336099100> PMID: 14603034
16. Tempera I, De Leo A, Kossenkov AV, Cesaroni M, Song H, Dawany N, et al. Identification of MEF2B, EBF1, and IL6R as Direct Gene Targets of Epstein-Barr Virus (EBV) Nuclear Antigen 1 Critical for EBV-Infected B-Lymphocyte Survival. *Journal of Virology*. 2016; 90(1):345–55. <https://doi.org/10.1128/JVI.02318-15> PMID: 26468528

17. Ballestas ME, Chatis PA, Kaye KM. Efficient persistence of extrachromosomal KSHV DNA mediated by latency-associated nuclear antigen. *Science*. 1999; 284(5414):641–4. Epub 1999/04/24. <https://doi.org/10.1126/science.284.5414.641> PMID: 10213686.
18. Hammerschmidt W, Sugden B. Identification and characterization of oriLyt, a lytic origin of DNA replication of Epstein-Barr virus. *Cell*. 1988; 55(3):427–33. Epub 1988/11/04. [https://doi.org/10.1016/0092-8674\(88\)90028-1](https://doi.org/10.1016/0092-8674(88)90028-1) PMID: 2846181.
19. van Santen V, Cheung A, Kieff E. Epstein-Barr virus RNA VII: size and direction of transcription of virus-specified cytoplasmic RNAs in a transformed cell line. *Proc Natl Acad Sci U S A*. 1981; 78(3):1930–4. Epub 1981/03/01. <https://doi.org/10.1073/pnas.78.3.1930> PMID: 6112750; PubMed Central PMCID: PMC319249.
20. Brooks LA, Lear AL, Young LS, Rickinson AB. Transcripts from the Epstein-Barr virus BamHI A fragment are detectable in all three forms of virus latency. *J Virol*. 1993; 67(6):3182–90. Epub 1993/06/01. <https://doi.org/10.1128/JVI.67.6.3182-3190.1993> PMID: 8388496; PubMed Central PMCID: PMC237657.
21. Ungerleider N, Concha M, Lin Z, Roberts C, Wang X, Cao S, et al. The Epstein Barr virus circRNAome. *PLoS Pathog*. 2018; 14(8):e1007206. <https://doi.org/10.1371/journal.ppat.1007206> PMID: 30080890.
22. Toptan T, Abere B, Nalesnik MA, Swerdlow SH, Ranganathan S, Lee N, et al. Circular DNA tumor viruses make circular RNAs. *Proc Natl Acad Sci U S A*. 2018; 115(37):E8737–E45. Epub 2018/08/29. <https://doi.org/10.1073/pnas.1811728115> PMID: 30150410; PubMed Central PMCID: PMC6140489.
23. Bullard WL, Flemington EK, Renne R, Tibbetts SA. Connivance, Complicity, or Collusion? The Role of Noncoding RNAs in Promoting Gammaherpesvirus Tumorigenesis. *Trends Cancer*. 2018; 4(11):729–40. Epub 2018/10/26. <https://doi.org/10.1016/j.trecan.2018.09.005> PMID: 30352676; PubMed Central PMCID: PMC6317380.
24. Bartel DP. Metazoan MicroRNAs. *Cell*. 2018; 173(1):20–51. Epub 2018/03/24. <https://doi.org/10.1016/j.cell.2018.03.006> PMID: 29570994; PubMed Central PMCID: PMC6091663.
25. Liu W, Wang X. Prediction of functional microRNA targets by integrative modeling of microRNA binding and target expression data. *Genome Biology*. 2019; 20(1). <https://doi.org/10.1186/s13059-019-1629-z> PMID: 30670076
26. Hu W, Dooley J, Chung SS, Chandramohan D, Cimmino L, Mukherjee S, et al. miR-29a maintains mouse hematopoietic stem cell self-renewal by regulating Dnmt3a. *Blood*. 2015; 125(14):2206–16. Epub 2015/01/31. <https://doi.org/10.1182/blood-2014-06-585273> PMID: 25634742; PubMed Central PMCID: PMC4383797.
27. Choi YJ, Lin CP, Ho JJ, He X, Okada N, Bu P, et al. miR-34 miRNAs provide a barrier for somatic cell reprogramming. *Nat Cell Biol*. 2011; 13(11):1353–60. Epub 2011/10/25. <https://doi.org/10.1038/ncb2366> PMID: 22020437; PubMed Central PMCID: PMC3541684.
28. Welch C, Chen Y, Stallings RL. MicroRNA-34a functions as a potential tumor suppressor by inducing apoptosis in neuroblastoma cells. *Oncogene*. 2007; 26(34):5017–22. Epub 2007/02/14. <https://doi.org/10.1038/sj.onc.1210293> PMID: 17297439.
29. Lu LF, Boldin MP, Chaudhry A, Lin LL, Taganov KD, Hanada T, et al. Function of miR-146a in controlling Treg cell-mediated regulation of Th1 responses. *Cell*. 2010; 142(6):914–29. Epub 2010/09/21. <https://doi.org/10.1016/j.cell.2010.08.012> PMID: 20850013; PubMed Central PMCID: PMC3049116.
30. Rodriguez A, Vigorito E, Clare S, Warren MV, Couttet P, Soond DR, et al. Requirement of bic/microRNA-155 for normal immune function. *Science*. 2007; 316(5824):608–11. Epub 2007/04/28. <https://doi.org/10.1126/science.1139253> PMID: 17463290; PubMed Central PMCID: PMC2610435.
31. Zhu JY, Pfuhl T, Motsch N, Barth S, Nicholls J, Grasser F, et al. Identification of novel Epstein-Barr virus microRNA genes from nasopharyngeal carcinomas. *J Virol*. 2009; 83(7):3333–41. Epub 2009/01/16. <https://doi.org/10.1128/JVI.01689-08> PMID: 19144710; PubMed Central PMCID: PMC2655542.
32. Grundhoff A, Sullivan CS, Ganem D. A combined computational and microarray-based approach identifies novel microRNAs encoded by human gamma-herpesviruses. *RNA*. 2006; 12(5):733–50. Epub 2006/03/17. <https://doi.org/10.1261/rna.2326106> PMID: 16540699; PubMed Central PMCID: PMC1440911.
33. Zhu JY, Strehle M, Frohn A, Kremmer E, Hofig KP, Meister G, et al. Identification and Analysis of Expression of Novel MicroRNAs of Murine Gammaherpesvirus 68. 2010; 84(19):10266–75. <https://doi.org/10.1128/JVI.01119-10> PMID: 20668074
34. Kozomara A, Birgaoanu M, Griffiths-Jones S. miRBase: from microRNA sequences to function. *Nucleic Acids Research*. 2019; 47(D1):D155–D62. <https://doi.org/10.1093/nar/gky1141> PMID: 30423142
35. Skalsky RL, Corcoran DL, Gottwein E, Frank CL, Kang D, Hafner M, et al. The viral and cellular microRNA targetome in lymphoblastoid cell lines. *PLoS Pathog*. 2012; 8(1):e1002484. Epub 2012/02/01.

- <https://doi.org/10.1371/journal.ppat.1002484> PMID: 22291592; PubMed Central PMCID: PMC3266933.
36. Haecker I, Gay LA, Yang Y, Hu J, Morse AM, McIntyre LM, et al. Ago HITS-CLIP expands understanding of Kaposi's sarcoma-associated herpesvirus miRNA function in primary effusion lymphomas. *PLoS Pathog.* 2012; 8(8):e1002884. Epub 2012/08/29. <https://doi.org/10.1371/journal.ppat.1002884> PMID: 22927820; PubMed Central PMCID: PMC3426530.
 37. Gottwein E, Corcoran DL, Mukherjee N, Skalsky RL, Hafner M, Nusbaum JD, et al. Viral microRNA targetome of KSHV-infected primary effusion lymphoma cell lines. *Cell Host Microbe.* 2011; 10(5):515–26. Epub 2011/11/22. <https://doi.org/10.1016/j.chom.2011.09.012> PMID: 22100165; PubMed Central PMCID: PMC3222872.
 38. Kang D, Skalsky RL, Cullen BR. EBV BART MicroRNAs Target Multiple Pro-apoptotic Cellular Genes to Promote Epithelial Cell Survival. *PLoS Pathog.* 2015; 11(6):e1004979. Epub 2015/06/13. <https://doi.org/10.1371/journal.ppat.1004979> PMID: 26070070; PubMed Central PMCID: PMC4466530.
 39. Barth S, Pfuhl T, Mamiani A, Ehses C, Roemer K, Kremmer E, et al. Epstein-Barr virus-encoded microRNA miR-BART2 down-regulates the viral DNA polymerase BALF5. *Nucleic Acids Res.* 2008; 36(2):666–75. Epub 2007/12/13. <https://doi.org/10.1093/nar/gkm1080> PMID: 18073197; PubMed Central PMCID: PMC2241876.
 40. Hooykaas MJG, van Gent M, Soppe JA, Kruse E, Boer IGJ, van Leenen D, et al. EBV MicroRNA BART16 Suppresses Type I IFN Signaling. *J Immunol.* 2017; 198(10):4062–73. Epub 2017/04/19. <https://doi.org/10.4049/jimmunol.1501605> PMID: 28416598.
 41. Helwak A, Kudla G, Dudnakova T, Tollervey D. Mapping the human miRNA interactome by CLASH reveals frequent noncanonical binding. *Cell.* 2013; 153(3):654–65. <https://doi.org/10.1016/j.cell.2013.03.043> PMID: 23622248; PubMed Central PMCID: PMC3650559.
 42. Gay LA, Sethuraman S, Thomas M, Turner PC, Renne R. Modified Cross-Linking, Ligation, and Sequencing of Hybrids (qCLASH) Identifies Kaposi's Sarcoma-Associated Herpesvirus MicroRNA Targets in Endothelial Cells. *J Virol.* 2018; 92(8). Epub 2018/02/02. <https://doi.org/10.1128/JVI.02138-17> PMID: 29386283; PubMed Central PMCID: PMC5874430.
 43. Grossman RL, Heath AP, Ferretti V, Varmus HE, Lowy DR, Kibbe WA, et al. Toward a Shared Vision for Cancer Genomic Data. *New England Journal of Medicine.* 2016; 375(12):1109–12. <https://doi.org/10.1056/nejmp1607591> PMID: 27653561
 44. Frankish A, Diekhans M, Ferreira A-M, Johnson R, Jungreis I, Loveland J, et al. GENCODE reference annotation for the human and mouse genomes. *Nucleic Acids Research.* 2019; 47(D1):D766–D73. <https://doi.org/10.1093/nar/gky955> PMID: 30357393
 45. O'Grady T, Wang X, Honer Zu Bentrup K, Baddoo M, Concha M, Flemington EK. Global transcript structure resolution of high gene density genomes through multi-platform data integration. *Nucleic Acids Res.* 2016; 44(18):e145. <https://doi.org/10.1093/nar/gkw629> PMID: 27407110; PubMed Central PMCID: PMC5062983.
 46. Bray NL, Pimentel H, Melsted P, Pachter L. Near-optimal probabilistic RNA-seq quantification. *Nature Biotechnology.* 2016; 34(5):525–7. <https://doi.org/10.1038/nbt.3519> PMID: 27043002
 47. Grande BM, Gerhard DS, Jiang A, Griner NB, Abramson JS, Alexander TB, et al. Genome-wide discovery of somatic coding and noncoding mutations in pediatric endemic and sporadic Burkitt lymphoma. *Blood.* 2019; 133(12):1313–24. <https://doi.org/10.1182/blood-2018-09-871418> PMID: 30617194
 48. Cristescu R, Lee J, Nebozhyn M, Kim K-M, Ting JC, Wong SS, et al. Molecular analysis of gastric cancer identifies subtypes associated with distinct clinical outcomes. *Nature Medicine.* 2015; 21(5):449–56. <https://doi.org/10.1038/nm.3850> PMID: 25894828
 49. Androvic P, Valihrach L, Elling J, Sjoback R, Kubista M. Two-tailed RT-qPCR: a novel method for highly accurate miRNA quantification. *Nucleic Acids Research.* 2017; 45(15):e144–e. <https://doi.org/10.1093/nar/gkx588> PMID: 28911110
 50. Love MI, Huber W, Anders S. Moderated estimation of fold change and dispersion for RNA-seq data with DESeq2. *Genome Biology.* 2014; 15(12). <https://doi.org/10.1186/s13059-014-0550-8> PMID: 25516281
 51. Huber W, Von Heydebreck A, Sultmann H, Poustka A, Vingron M. Variance stabilization applied to microarray data calibration and to the quantification of differential expression. *Bioinformatics.* 2002; 18(Suppl 1):S96–S104. https://doi.org/10.1093/bioinformatics/18.suppl_1.s96 PMID: 12169536
 52. McFadden D. Conditional logic analysis of qualitative choice behavior. [Berkeley]: [Institute of Urban & Regional Development, University of California]; 1972.
 53. Szklarczyk D, Gable AL, Lyon D, Junge A, Wyder S, Huerta-Cepas J, et al. STRING v11: protein–protein association networks with increased coverage, supporting functional discovery in genome-wide

- experimental datasets. *Nucleic Acids Research*. 2019; 47(D1):D607–D13. <https://doi.org/10.1093/nar/gky1131> PMID: 30476243
54. Kuleshov MV, Jones MR, Rouillard AD, Fernandez NF, Duan Q, Wang Z, et al. Enrichr: a comprehensive gene set enrichment analysis web server 2016 update. *Nucleic Acids Research*. 2016; 44(W1):W90–W7. <https://doi.org/10.1093/nar/gkw377> PMID: 27141961
 55. Dalla-Favera R, Bregni M, Erikson J, Patterson D, Gallo RC, Croce CM. Human c-myc onc gene is located on the region of chromosome 8 that is translocated in Burkitt lymphoma cells. *Proceedings of the National Academy of Sciences*. 1982; 79(24):7824–7. <https://doi.org/10.1073/pnas.79.24.7824> PMID: 6961453
 56. Neel BG, Jhanwar SC, Chaganti RS, Hayward WS. Two human c-onc genes are located on the long arm of chromosome 8. 1982; 79(24):7842–6. <https://doi.org/10.1073/pnas.79.24.7842> PMID: 6961456
 57. TCGA. Comprehensive molecular characterization of gastric adenocarcinoma. *Nature*. 2014; 513(7517):202–9. <https://doi.org/10.1038/nature13480> PMID: 25079317
 58. Van Cutsem E, Sagaert X, Topal B, Haustermans K, Prenen H. Gastric cancer. *The Lancet*. 2016; 388(10060):2654–64. [https://doi.org/10.1016/s0140-6736\(16\)30354-3](https://doi.org/10.1016/s0140-6736(16)30354-3)
 59. Cancer Genome Atlas Research N. Comprehensive molecular characterization of gastric adenocarcinoma. *Nature*. 2014; 513(7517):202–9. Epub 2014/08/01. <https://doi.org/10.1038/nature13480> PMID: 25079317; PubMed Central PMCID: PMC4170219.
 60. Brown BD, Gentner B, Cantore A, Colleoni S, Amendola M, Zingale A, et al. Endogenous microRNA can be broadly exploited to regulate transgene expression according to tissue, lineage and differentiation state. 2007; 25(12):1457–67. <https://doi.org/10.1038/nbt1372> PMID: 18026085
 61. Ma L, Teruya-Feldstein J, Weinberg RA. Tumour invasion and metastasis initiated by microRNA-10b in breast cancer. *Nature*. 2007; 449(7163):682–8. <https://doi.org/10.1038/nature06174> PMID: 17898713
 62. Flores O, Kennedy EM, Skalsky RL, Cullen BR. Differential RISC association of endogenous human microRNAs predicts their inhibitory potential. *Nucleic acids research*. 2014; 42(7):4629–39. Epub 2014/01/23. <https://doi.org/10.1093/nar/gkt1393> PMID: 24464996.
 63. Helwak A, Kudla G, Dudnakova T, Tollervey D. Mapping the Human miRNA Interactome by CLASH Reveals Frequent Noncanonical Binding. *Cell*. 2013; 153(3):654–65. <https://doi.org/10.1016/j.cell.2013.03.043> PMID: 23622248
 64. Yang YC, Liem A, Lambert PF, Sugden B. Dissecting the regulation of EBV's BART miRNAs in carcinomas. *Virology*. 2017; 505:148–54. Epub 2017/03/05. <https://doi.org/10.1016/j.virol.2017.02.013> PMID: 28259048; PubMed Central PMCID: PMC5504693.
 65. Qiu J, Smith P, Leahy L, Thorley-Lawson DA. The Epstein-Barr virus encoded BART miRNAs potentiate tumor growth in vivo. *PLoS Pathog*. 2015; 11(1):e1004561. <https://doi.org/10.1371/journal.ppat.1004561> PMID: 25590614; PubMed Central PMCID: PMC4295875.
 66. Bullard WL, Kara M, Gay LA, Sethuraman S, Wang Y, Nirmalan S, et al. Identification of murine gammaherpesvirus 68 miRNA-mRNA hybrids reveals miRNA target conservation among gammaherpesviruses including host translation and protein modification machinery. *PLOS Pathogens*. 2019; 15(8):e1007843. <https://doi.org/10.1371/journal.ppat.1007843> PMID: 31393953
 67. Feldman ER, Kara M, Oko LM, Grau KR, Krueger BJ, Zhang J, et al. A Gammaherpesvirus Noncoding RNA Is Essential for Hematogenous Dissemination and Establishment of Peripheral Latency. *mSphere*. 2016; 1(2). Epub 2016/03/02. <https://doi.org/10.1128/mSphere.00105-15> PMID: 27110595; PubMed Central PMCID: PMC4838037.
 68. Arvey A, Larsson E, Sander C, Leslie CS, Marks DS. Target mRNA abundance dilutes microRNA and siRNA activity. 2010; 6. <https://doi.org/10.1038/msb.2010.24> PMID: 20404830
 69. Schirle NT, Sheu-Gruttadauria J, Macrae IJ. Structural basis for microRNA targeting. *Science*. 2014; 346(6209):608–13. <https://doi.org/10.1126/science.1258040> PMID: 25359968
 70. McGeary SE, Lin KS, Shi CY, Pham TM, Bisaria N, Kelley GM, et al. The biochemical basis of microRNA targeting efficacy. *Science*. 2019; 366(6472):eaav1741. <https://doi.org/10.1126/science.aav1741> PMID: 31806698
 71. Ameres SL, Martinez J, Schroeder R. Molecular Basis for Target RNA Recognition and Cleavage by Human RISC. *Cell*. 2007; 130(1):101–12. <https://doi.org/10.1016/j.cell.2007.04.037> PMID: 17632058
 72. Bernhart SH, Hofacker IL, Stadler PF. Local RNA base pairing probabilities in large sequences. *Bioinformatics*. 2006; 22(5):614–5. <https://doi.org/10.1093/bioinformatics/btk014> PMID: 16368769
 73. Garcia DM, Baek D, Shin C, Bell GW, Grimson A, Bartel DP. Weak seed-pairing stability and high target-site abundance decrease the proficiency of Isy-6 and other microRNAs. *Nature Structural & Molecular Biology*. 2011; 18(10):1139–46. <https://doi.org/10.1038/nsmb.2115> PMID: 21909094

74. Strong MJ, Xu G, Coco J, Baribault C, Vinay DS, Lacey MR, et al. Differences in gastric carcinoma microenvironment stratify according to EBV infection intensity: implications for possible immune adjuvant therapy. *PLoS Pathog.* 2013; 9(5):e1003341. <https://doi.org/10.1371/journal.ppat.1003341> PMID: 23671415; PubMed Central PMCID: PMC3649992.
75. Newman AM, Steen CB, Liu CL, Gentles AJ, Chaudhuri AA, Scherer F, et al. Determining cell type abundance and expression from bulk tissues with digital cytometry. *Nature Biotechnology.* 2019; 37(7):773–82. <https://doi.org/10.1038/s41587-019-0114-2> PMID: 31061481
76. Bolotin DA, Poslavsky S, Mitrophanov I, Shugay M, Mamedov IZ, Putintseva EV, et al. MiXCR: software for comprehensive adaptive immunity profiling. *Nature Methods.* 2015; 12(5):380–1. <https://doi.org/10.1038/nmeth.3364> PMID: 25924071
77. Shugay M, Bagaev DV, Turchaninova MA, Bolotin DA, Britanova OV, Putintseva EV, et al. VDJtools: Unifying Post-analysis of T Cell Receptor Repertoires. *PLoS Computational Biology.* 2015; 11(11): e1004503. <https://doi.org/10.1371/journal.pcbi.1004503> PMID: 26606115
78. Mootha VK, Lindgren CM, Eriksson K-F, Subramanian A, Sihag S, Lehar J, et al. PGC-1 α -responsive genes involved in oxidative phosphorylation are coordinately downregulated in human diabetes. *Nature Genetics.* 2003; 34(3):267–73. <https://doi.org/10.1038/ng1180> PMID: 12808457
79. Subramanian A, Tamayo P, Mootha VK, Mukherjee S, Ebert BL, Gillette MA, et al. Gene set enrichment analysis: a knowledge-based approach for interpreting genome-wide expression profiles. *Proc Natl Acad Sci U S A.* 2005; 102(43):15545–50. Epub 2005/10/04. <https://doi.org/10.1073/pnas.0506580102> PMID: 16199517; PubMed Central PMCID: PMC1239896.
80. Farh KKH. The Widespread Impact of Mammalian MicroRNAs on mRNA Repression and Evolution. *Science.* 2005; 310(5755):1817–21. <https://doi.org/10.1126/science.1121158> PMID: 16308420
81. Simkin A, Geissler R, McIntyre ABR, Grimson A. Evolutionary dynamics of microRNA target sites across vertebrate evolution. *PLOS Genetics.* 2020; 16(2):e1008285. <https://doi.org/10.1371/journal.pgen.1008285> PMID: 32012152
82. Agarwal V, Bell GW, Nam J-W, Bartel DP. Predicting effective microRNA target sites in mammalian mRNAs. *eLife.* 2015; 4. <https://doi.org/10.7554/eLife.05005> PMID: 26267216
83. Hafner M, Landthaler M, Burger L, Khorshid M, Hausser J, Berninger P, et al. Transcriptome-wide identification of RNA-binding protein and microRNA target sites by PAR-CLIP. *Cell.* 2010; 141(1):129–41. Epub 2010/04/08. <https://doi.org/10.1016/j.cell.2010.03.009> PMID: 20371350; PubMed Central PMCID: PMC2861495.
84. Mishra R, Kumar A, Ingle H, Kumar H. The Interplay Between Viral-Derived miRNAs and Host Immunity During Infection. *Frontiers in Immunology.* 2020; 10. <https://doi.org/10.3389/fimmu.2019.03079> PMID: 32038626
85. Choy EY-W, Siu K-L, Kok K-H, Lung RW-M, Tsang CM, To K-F, et al. An Epstein-Barr virus–encoded microRNA targets PUMA to promote host cell survival. 2008; 205(11):2551–60. <https://doi.org/10.1084/jem.20072581> PMID: 18838543
86. Kim H, Choi H, Lee SK. Epstein-Barr Virus MicroRNA miR-BART20-5p Suppresses Lytic Induction by Inhibiting BAD-Mediated caspase-3-Dependent Apoptosis. 2016; 90(3):1359–68. <https://doi.org/10.1128/JVI.02794-15> PMID: 26581978
87. Kanda T, Miyata M, Kano M, Kondo S, Yoshizaki T, Iizasa H. Clustered MicroRNAs of the Epstein-Barr Virus Cooperatively Downregulate an Epithelial Cell-Specific Metastasis Suppressor. *Journal of Virology.* 2015; 89(5):2684–97. <https://doi.org/10.1128/JVI.03189-14> PMID: 25520514
88. Nachmani D, Stern-Ginossar N, Sarid R, Mandelboim O. Diverse herpesvirus microRNAs target the stress-induced immune ligand MICB to escape recognition by natural killer cells. *Cell Host Microbe.* 2009; 5(4):376–85. <https://doi.org/10.1016/j.chom.2009.03.003> PMID: 19380116.
89. Tagawa T, Albanese M, Bouvet M, Moosmann A, Mautner J, Heissmeyer V, et al. Epstein-Barr viral miRNAs inhibit antiviral CD4+ T cell responses targeting IL-12 and peptide processing. *The Journal of Experimental Medicine.* 2016; 213(10):2065–80. <https://doi.org/10.1084/jem.20160248> PMID: 27621419
90. Klinke O, Feederle R, Delecluse H-J. Genetics of Epstein-Barr virus microRNAs. *Seminars in Cancer Biology.* 2014; 26:52–9. <https://doi.org/10.1016/j.semcancer.2014.02.002> PMID: 24602823
91. Dolken L, Malterer G, Erhard F, Kothe S, Friedel CC, Suffert G, et al. Systematic analysis of viral and cellular microRNA targets in cells latently infected with human gamma-herpesviruses by RISC immunoprecipitation assay. *Cell Host Microbe.* 2010; 7(4):324–34. Epub 2010/04/24. <https://doi.org/10.1016/j.chom.2010.03.008> PMID: 20413099.
92. Yu Z, Chen T, Li X, Yang M, Tang S, Zhu X, et al. Lys29-linkage of ASK1 by Skp1-Cullin1-Fbxo21 ubiquitin ligase complex is required for antiviral innate response. *eLife.* 2016; 5. <https://doi.org/10.7554/eLife.14087> PMID: 27063938

93. Lang X, Tang T, Jin T, Ding C, Zhou R, Jiang W. TRIM65-catalyzed ubiquitination is essential for MDA5-mediated antiviral innate immunity. *The Journal of Experimental Medicine*. 2017; 214(2):459–73. <https://doi.org/10.1084/jem.20160592> PMID: 28031478
94. Li Q, Yan J, Mao AP, Li C, Ran Y, Shu HB, et al. Tripartite motif 8 (TRIM8) modulates TNF—and IL-1-triggered NF- κ B activation by targeting TAK1 for K63-linked polyubiquitination. *Proceedings of the National Academy of Sciences*. 2011; 108(48):19341–6. <https://doi.org/10.1073/pnas.1110946108> PMID: 22084099
95. Albanese M, Tagawa T, Bouvet M, Maliqi L, Lutter D, Hoser J, et al. Epstein–Barr virus microRNAs reduce immune surveillance by virus-specific CD8⁺T cells. *Proceedings of the National Academy of Sciences*. 2016; 113(42):E6467–E75. <https://doi.org/10.1073/pnas.1605884113> PMID: 27698133
96. Murer A, Rühl J, Zbinden A, Capaul R, Hammerschmidt W, Chijioke O, et al. MicroRNAs of Epstein–Barr Virus Attenuate T-Cell-Mediated Immune Control In Vivo. *mBio*. 2019; 10(1). <https://doi.org/10.1128/mbio.01941-18> PMID: 30647153
97. Le Gall S, Erdtmann L, Benichou S, Berlioz-Torrent C, Liu L, Benarous R, et al. Nef interacts with the mu subunit of clathrin adaptor complexes and reveals a cryptic sorting signal in MHC I molecules. *Immunity*. 1998; 8(4):483–95. Epub 1998/05/20. [https://doi.org/10.1016/s1074-7613\(00\)80553-1](https://doi.org/10.1016/s1074-7613(00)80553-1) PMID: 9586638.
98. Hu Z, Zhang Z, Doo E, Coux O, Goldberg AL, Liang TJ. Hepatitis B virus X protein is both a substrate and a potential inhibitor of the proteasome complex. *J Virol*. 1999; 73(9):7231–40. Epub 1999/08/10. <https://doi.org/10.1128/JVI.73.9.7231-7240.1999> PMID: 10438810; PubMed Central PMCID: PMC104247.
99. Coscoy L, Ganem D. Kaposi's sarcoma-associated herpesvirus encodes two proteins that block cell surface display of MHC class I chains by enhancing their endocytosis. *Proceedings of the National Academy of Sciences*. 2000; 97(14):8051–6. <https://doi.org/10.1073/pnas.140129797> PMID: 10859362
100. Boname JM, Stevenson PG. MHC Class I Ubiquitination by a Viral PHD/LAP Finger Protein. *Immunity*. 2001; 15(4):627–36. [https://doi.org/10.1016/s1074-7613\(01\)00213-8](https://doi.org/10.1016/s1074-7613(01)00213-8) PMID: 11672544
101. Ahn K, Gruhler A, Galocha B, Jones TR, Wiertz EJHJ, Ploegh HL, et al. The ER-Luminal Domain of the HCMV Glycoprotein US6 Inhibits Peptide Translocation by TAP. *Immunity*. 1997; 6(5):613–21. [https://doi.org/10.1016/s1074-7613\(00\)80349-0](https://doi.org/10.1016/s1074-7613(00)80349-0) PMID: 9175839
102. Horst D, Van Leeuwen D, Croft NP, Garstka MA, Hislop AD, Kremmer E, et al. Specific Targeting of the EBV Lytic Phase Protein BNLF2a to the Transporter Associated with Antigen Processing Results in Impairment of HLA Class I-Restricted Antigen Presentation. *The Journal of Immunology*. 2009; 182(4):2313–24. <https://doi.org/10.4049/jimmunol.0803218> PMID: 19201886
103. Raftery MJ, Schwab M, Eibert SM, Samstg Y, Walczak H, Schönrich G. Targeting the Function of Mature Dendritic Cells by Human Cytomegalovirus. 2001; 15(6):997–1009. [https://doi.org/10.1016/s1074-7613\(01\)00239-4](https://doi.org/10.1016/s1074-7613(01)00239-4) PMID: 11754820
104. McGranahan N, Furness AJS, Rosenthal R, Ramskov S, Lyngaa R, Saini SK, et al. Clonal neoantigens elicit T cell immunoreactivity and sensitivity to immune checkpoint blockade. *Science*. 2016; 351(6280):1463–9. <https://doi.org/10.1126/science.aaf1490> PMID: 26940869
105. Yang Y-C, Liem A, Lambert PF, Sugden B. Dissecting the regulation of EBV's BART miRNAs in carcinomas. 2017; 505:148–54. <https://doi.org/10.1016/j.virol.2017.02.013> PMID: 28259048
106. Ungerleider N, Flemington E. SpliceV: analysis and publication quality printing of linear and circular RNA splicing, expression and regulation. *BMC Bioinformatics*. 2019; 20(1):231. Epub 2019/05/10. <https://doi.org/10.1186/s12859-019-2865-7> PMID: 31068132; PubMed Central PMCID: PMC6507234.
107. Lorenz R, Bernhart SH, Höner Zu Siederdisen C, Tafer H, Flamm C, Stadler PF, et al. ViennaRNA Package 2.0. *Algorithms for Molecular Biology*. 2011; 6(1):26. <https://doi.org/10.1186/1748-7188-6-26> PMID: 22115189
108. Grimson A, Farh KK-H, Johnston WK, Garrett-Engle P, Lim LP, Bartel DP. MicroRNA Targeting Specificity in Mammals: Determinants beyond Seed Pairing. *Molecular Cell*. 2007; 27(1):91–105. <https://doi.org/10.1016/j.molcel.2007.06.017> PMID: 17612493
109. Ramasubramanian S, Osborn K, Al-Mohammad R, Ijuel B, Zuo J, Balan N, et al. Epstein–Barr virus transcription factor Zta acts through distal regulatory elements to directly control cellular gene expression. *Nucleic Acids Research*. 2015; 43(7):3563–77. <https://doi.org/10.1093/nar/gkv212> PMID: 25779048
110. Langmead B, Salzberg SL. Fast gapped-read alignment with Bowtie 2. *Nature Methods*. 2012; 9(4):357–9. <https://doi.org/10.1038/nmeth.1923> PMID: 22388286
111. Travis AJ, Moody J, Helwak A, Tollervey D, Kudla G. Hyb: a bioinformatics pipeline for the analysis of CLASH (crosslinking, ligation and sequencing of hybrids) data. *Methods*. 2014; 65(3):263–73. Epub

2013/11/12. <https://doi.org/10.1016/j.ymeth.2013.10.015> PMID: [24211736](https://pubmed.ncbi.nlm.nih.gov/24211736/); PubMed Central PMCID: [PMC3969109](https://pubmed.ncbi.nlm.nih.gov/PMC3969109/).